PHYSICAL REVIEW B VOLUME 44, NUMBER 8 15 AUGUST 1991-II

Electronic structure of NiO: Correlation and band effects

Z.-X. Shen
Stanford Electronics Laboratory, Stanford University, Stanford, California 94305

R. S. List
Los Alamos National Laboratory, Los Alamos, New Mexico 87545

D. S. Dessau and B. O. Wells
Stanford Electronics Laboratory, Stanford University, Stanford, California 94305

O. Jepsen
Max-Planck-Institute for Solid State Research, D-7000 Stuttgart 80, Federal Republic of Germany

A. J. Arko and R. Barttlet
Los Alamos National Laboratory, Los Alamos, New Mexico 87545

C. K. Shih
Department of Physics, University of Texas, Austin, Texas 78712

F. Parmigiani
IBM Research Division, Almaden Research Center, 650 Harry Road, San Jose, California 95120

J. C. Huang and P. A. P. Lindberg
Stanford Electronics Laboratory, Stanford University, Stanford, California 94305
(Received 4 September 1990; revised manuscript received 23 January 1991)

We have performed angle-resolved-photoemission experiments and local-density-functional (LDA) band calculations on NiO to study correlation and band effects of this conceptually important compound. Our experimental result suggests a dual nature of the electronic structure of NiO. On the one hand, the LDA band calculation has some relevance to the electronic structure of NiO, and the inclusion of the antiferromagnetic order is essential. For the lower O $2p$ bands, the LDA calculation agrees almost perfectly with experimental energy positions and dispersion relations. On the other hand, discrepancies between the experiment and the LDA calculation do exist, especially for the Ni $3d$ bands and the O $2p$ bands that are heavily mixed with the Ni $3d$ bands. It appears that the main discrepancies between the experimental results and the LDA calculation are concentrated in the regions of the insulating gap and the valence-band satellite. In addition to these results, we also report the interesting angle and photon-energy dependence of the satellite emission. The above results show that the angle-resolved-photoemission studies can provide much additional information about the electronic structure of correlated materials like NiO.

I. INTRODUCTION

In two recent short papers, we have briefly reported some of our recent angle-resolved-photoemission studies of NiO.[1,2] The primary issues we discussed were the effects of both correlation and translational symmetry, the influence of antiferromagnetic order on the electronic structure, as well as the experimental observation of energy dispersions of the valence-band satellite. In this paper, we provide more detailed information about these important issues.

The electronic structure of NiO has three interesting aspects: the correlation effect as a result of the strong Coulomb interaction, the band effect as a result of the translational symmetry, and the influence of the antiferromagnetic order (which is another form of the interesting correlation effects and is related with the large Coulomb interaction). Among the three interesting aspects of the electronic structure of NiO, the correlation effect due to the large Coulomb U has previously been the most extensively studied issue.

Because of its correlated nature as a result of the large Coulomb U, NiO has continuously been at the center of the controversy between the localized Mott-Hubbard picture and the one-electron band picture for a class of materials often called Mott insulators.[3–5] As is well known, one milestone in modern solid-state physics was the development of the one-electron band theory which reduces the complicated many-body physics problem of the real solid into a problem of a single electron in the average potential of ions and other electrons.[6–8] For years, band

theory has proven to be very successful in explaining many physical and chemical properties of a large class of solid materials, especially for simple metals and semiconductors. Band theory also provides us with the basic concept of metals and insulators: a metal corresponds to a material which has a partially filled band, while an insulator corresponds to a material which has a gap between filled bands and empty bands.

However, it was recognized soon after the invention of the band theory that a certain class of materials (represented by NiO and other transition-metal monooxides) cannot be described by the simple band theory. According to the band theory, they should be metals, but are experimentally found to be insulators. This problem of band theory has been a focal point of condensed-matter physics research for a long time.[3-5] Currently, two very different view points exist to explain this problem, leading to great controversy. On the one hand, Mott, Hubbard, and Anderson have argued that this failure of the one-electron picture to predict an insulating nature for these oxides is due to the intrinsic limitation of the one-electron approach. These materials are strongly correlated because of strong Coulomb interaction among the $3d$ electrons, so that the one-electron approximation breaks down.[9-11] Based on a simple hydrogenlike model, Mott illustrated that the simple band picture breaks down and a gap opens when the Coulomb interaction energy (U) is larger than the bandwidth (W).[9] This is why these oxides are often called Mott insulators.

On the other hand, Slater argued that this failure of the one-electron band theory to predict an insulating ground state was related to certain approximations in the calculation, but was not because of the band theory itself.[12] He recognized that a Mott insulator often has an antiferromagnetic order below its Neel temperature; therefore, this magnetic order should be included in the calculation. This is the so-called Slater antiferromagnetism approach or the spin-polarized band calculation.[13,14] In fact, some recent sophisticated spin-polarized band calculations give small gaps for materials like NiO,[13] and this was regarded as a demonstration of the success of the one-electron band theory.[13] However, even though the calculation gave some correct answers for the ground-state properties of NiO (not for the magnetic moment, though) it predicted a gap value of 0.2 eV, which is an order of magnitude smaller than the experimental value of about 4 eV.[15,16] This problem with the band gap has been a major difficulty in attempts to describe NiO with band theory.

During the last decade, photoelectron spectroscopy (PES) was extensively used to understand the excited properties of the transition-metal mono-oxides.[16-28] Based on results of spectroscopic data, Sawatzky and Allen, Fujimori and Minani revised the Mott-Hubbard description of these insulators.[16,17] In this revised picture, the p-d charge transfer which involves the energy Δ is considered, as well as the d-d charge fluctuation which involves the Coulomb energy U. Therefore, as a first-order approximation, we have the following picture for the insulator: the localized $3d$ bands are split into the upper and the lower Hubbard bands separated by the Coulomb energy U with the lower Hubbard band filled and the upper Hubbard band empty. The oxygen band resides in between the upper and lower Hubbard band and forms a charge transfer gap with the upper Hubbard band. An important piece of spectroscopic evidence to support this revised picture of NiO is the existence of the valence-band satellite and its resonance behavior near the Ni $3p$-to-$3d$ absorption edge.[19,20,29] This picture of NiO has been widely accepted with few exceptions.[30] Since the discovery of the high-temperature superconductors, this same picture of Mott insulators was extensively used to interpret the spectroscopic data,[31-34] and to construct microscopic models for the cuprate superconductors.[35]

Unlike the correlation effect, both the band effect due to the translational symmetry and the influence of the antiferromagnetic order on the electronic structure remain basically unexplored experimentally. To the best of our knowledge, no real angle-resolved-photoemission experiments have been performed on NiO to study the band effect until our recent studies.[1,2,36] The effects of the influence of the antiferromagnetic order on the electronic structure have never been explicitly addressed experimentally.

The purpose of this detailed angle-resolved-photoemission study of NiO is to address these three interesting aspects of the electronic structure in a coherent way. Our approach was to compare the angle-resolved-photoemission data with the result of band calculations. We performed the experiment and the analysis of the data in the standard way, as one would do for simple noncorrelated materials. In this way, we could test the ability of the simple one-electron band theory to explain the electronic structure of NiO. We want to emphasize that the bands which we will call d-bands in our comparison with the band calculations are the bound states of mixed $d^8\underline{L}$, $d^9\underline{L}^2$, and d^7 characters in the cluster picture discussed in the last two paragraphs. Here $\underline{L}$ stands for a ligand hole. As will be discussed in detail in Sec. VII, we call those bands d bands only because it is easier for the comparison if we use the band language. To address the issue of the antiferromagnetic order more explicitly, we compared the experimentally obtained bands with results of both nonmagnetic and antiferromagnetic band calculations.

In general, our experimental data have given mixed results as to the correct description of the electronic structure of NiO: *both localized and band effects clearly exist in our experimental data.* On the one hand, the local-density-functional (LDA) band calculation certainly has some relevance to the electronic structure (as measured by photoemission) of NiO. It gives the essentially correct energy separations between the occupied Ni $3d$ and the O $2p$ bands. For the Ni $3d$ bands, the LDA calculation gives the basically correct relative energy positions of the individual bands. For the lower O $2p$ bands, the LDA calculation agrees almost perfectly with both the experimental energy positions and the dispersion relations. On the other hand, discrepancies between the experiment and the band calculation do exist. The main discrepancies between the experimental result and the LDA calculation appear to be concentrated in the energy regions of

the insulating gap and the valence-band satellite.

In addition, the comparison of our data with both the nonmagnetic and the antiferromagnetic bands unambiguously demonstrates that the inclusion of the antiferromagnetic order is essential for the electronic structure of NiO. The antiferromagnetic LDA bands agree with the experimental data significantly better than the nonmagnetic LDA bands. Finally, we have also made an interesting observation of the energy dispersion for the valence-band satellite, which is often regarded as a symbol of the localized nature of NiO. This again is consistent with the dual picture inferred from a direct comparison between the data and the band theory.

These experimental results show that angle-resolved-photoemission experiments can provide much new information about the electronic structure of materials like NiO. We hope this work will stimulate more angle-resolved-photoemission experiments on this and other Mott insulators, which will guide the theoretical efforts to improve our understanding of these conceptually important materials. As the same time, we also call for more theoretical efforts to account for the dual picture we have found here. This may involve either incorporating the correlation effects into the band calculations or incorporating the band effects into the localized models.

This paper is organized in the following way: In Sec. II, we give details of the experimental setup, theoretical calculation, and the method of analysis of the experimental data. In Sec. III, the normal emission data from NiO $\langle 100 \rangle$ are presented, and in Sec. IV, off-normal-emission data from NiO $\langle 100 \rangle$. In Sec. V, we show results of off-normal-emission experiments along NiO $\langle 110 \rangle$. In Sec. VI, we present the experimental observation of the energy dispersion of the valence-band satellite. In Sec. VII, we discuss our results. Section VIII contains the conclusions of our work.

II. EXPERIMENTAL AND CALCULATIONAL DETAILS

The angle-resolved-photoemission experiments were performed in three experimental runs at the Stanford Synchtrotron Radiation Laboratory (SSRL) at Stanford, California; the Synchrotron Radiation Center (SRC) at Stoughton, Wisconsin; and the National Synchrotron Light Source at Brookhaven, New York.

The experiments at SSRL were performed on the 18° Seya-Naminoka beam line III-2 with the photon energy ranging from 10 to 35 eV. The photoelectrons were collected and analyzed by a hemispherical energy analyzer with $\pm 2°$ angular resolution in a Vacuum Generator (VG) ADES 400 system. The single crystal of NiO was cleaved *in situ* (base pressure $< 2\times 10^{-10}$ Torr), and its (100) cleavage surface was verified by low-energy electron diffraction (LEED). The photoemission measurements were carried out at room temperature, which is well below the Neel temperature (T_N) of NiO (550 K). The surface normal of the crystal was determined by a laser beam, and the 45° photon incident angle was used in this case, giving relaxed selection rules. The combined energy resolution of both the analyzer and the monochromator was better than 0.3 eV.

The experiments at SRC were performed on the Minnesota/Argonne/Los Alamos extended-range grasshopper beam line with photon energies above 40 eV (all the data with photon energy larger than 40 eV were obtained during this run except for data in Figs. 19 and 20). The photoelectrons were collected and analyzed by a hemispherical energy analyzer with $\pm 1°$ angular resolution in a Vacuum Science Workshop (VSW) chamber. The single crystals of NiO were cleaved *in situ* with a base pressure better than 2×10^{-10} Torr. The measurements were again carried out at room temperature. The surface normal of the crystal was determined by laser light reflections. This was then verified by making sure that the spectra were symmetric about the normal. The (100) cleavage surface (which is the natural cleavage surface of NiO) was checked by its Laue pattern before and after the angle-resolved-photoemission experiments. The orientations of the two $\langle 100 \rangle$ axes within the (100) surface for off-normal-emission experiments were also determined by Laue prior to the photoemission measurements. Various photon incident angles were used in this case, which will be indicated in each of the individual data sets as they are presented. The combined energy resolution of the photon source and the spectrometer was about 0.15 eV for the data presented here. Even better energy resolution (0.08 eV) was tried, but that did not enhance our ability to resolve the details of the bands. This indicated that the intrinsic width of the bands are the resolutional limitation.

The experiments at Brookhaven were performed on the Los Alamos extended grasshopper beam line with photon energies above 40 eV. The same VSW chamber was used to perform the experiment (data presented in Figs. 19 and 20). The chamber base pressure was 3×10^{-10} Torr, and the experiments were performed at room temperature. The surface normal of the crystal in this case was determined by a laser. The overall energy resolution of the system in this case is 0.3 eV or better.

Because the energy bands along the directions we measured were not available in the literature, we had to recalculate them. The calculation and the experiment were carried out independently. These first-principles density-functional band-structure calculations used the local potential of von Barth and Hedin.[37] The calculation were performed by the scalar-relativistic self-consistent linear-muffin-tin-orbital method of Andersen in the atomic-spheres approximation including the combined correction term and with a minimal basis set in the standard way.[38,39] The calculated antiferromagnetic bands (AF II) are basically the same as the earlier result by Terakura and co-workers.[13] The largest difference is that in our calculation, the separation between the oxygen p bands and the nickel d bands is 0.2 eV smaller than in Ref. 13. This small discrepancy could be due to the fact that the somewhat different exchange-correlation potentials used in the two calculations differ in detail. The nonmagnetic band presented here is very different from the earlier non-self-consistent calculation.[40]

The standard data-analysis procedures for angle-resolved photoemission were used to extrapolate the E vs $\mathbf{k}$ relations of NiO.[41–45] The method of data analysis we

adapt here has been very extensively used in semiconductors and simple metals. In cases such as Cu and GaAs, this method has worked very well.[42,44] An important approximation is the use of free-electron final states, which is usually regarded as a fair approximation for photon energies higher than certain values [in the cases of Cu and GaAs, for example, the free-electron final-state approximation is regarded to be a good approximation for photon energies higher than 22 eV (Refs. 42, 44, and 45)]. Another point which is usually not explicitly assumed is that the peaks observed in the photoemission spectra are due to direct transitions (i.e., **k**-conserved transition) between the initial state and the final state. This is true only because the photon momentum is almost negligible, as compared with the momentum of the photoelectrons in the photon energy range used. Indirect transitions do occur in the photoemission spectra, but they are usually weak in intensity, and are often related with the so-called one-dimensional density of states.[44]

In the case of normal emission, the formula to calculate $\mathbf{k}_\perp$ is $k_\perp = 0.51\sqrt{m_e^*(E-E_0)}$. Here E is the energy of photoelectron reference to E_F, E_0 is the inner potential which usually is a fitting parameter, and m_e^* is the effective mass of the final state. In the calculation, we take $E_0 = -8$ eV, which is a very reasonable value for the inner potential,[44,45] and is consistent with an earlier study of CoO.[46] Therefore, E_0 can be regarded as a constrained fitting parameter. For the free-electron final-state approximation to be reasonable, the value of m_e^* should be roughly in the range of 0.8–1.2. In our case, we chose a value of 0.95 to fit the Γ point of the $\Delta 1$ oxygen band for our earlier normal-emission data;[1] we stick with this number for the sake of consistency. Our results are not very sensitive to small variations of m_e^* (e.g., all the conclusions remain the same if we change m_e from 0.95 to 1).

In the case of off-normal emission along $\langle 100 \rangle$, the formula to calculate the $\mathbf{k}_\parallel$ is $k_\parallel = 0.51\sqrt{m_e E_{\rm kin}}(\sin\theta)$. Here both $E_{\rm kin}$ and the emission angle θ are directly measurable quantities. A very important point here is that the inner potential value does not enter the relation directly. Therefore, this provides an important test on whether the inner potential value we have chosen for the normal emission data is reasonable or not. As will be shown later, the normal-emission data and the off-normal-emission data have excellent consistency, especially for the best determined $\Delta 1$ oxygen band. This consistency gives us confidence in our interpretation of the experimental data.

The off-normal-emission measurement on NiO has a complication that the normal-emission measurement does not. Because NiO is a three-dimensional material, we have to change the photon energy and the emission angle at the same time so that we can keep $\mathbf{k}_\perp$ constant. In this way, a direct comparison with the band calculation is possible. The off-normal-emission experiments along $\langle 110 \rangle$ were performed in two different geometries as illustrated in Fig. 1. The formulas for $\mathbf{k}_\parallel$ in the two cases are $k_\parallel = 0.51\sqrt{m_e E_{\rm kin}}(\sin\phi)\sqrt{2}$; $k_\parallel = 0.51\sqrt{m_e E_{kin}}(\sin\theta)$.

In all cases, the **k** value obtained is plotted out in units of $2\pi/a$, and a is the lattice constant of 4.18 Å. The experimental E vs **k** relations are plotted in the reduced zone scheme. If the data points are not inside the first Brillouin zone, they will be mapped back into the first zone. (In fact, many of our data points are in the second Brillouin zone.) Because NiO has the fcc structure, the length of the reciprocal lattice vectors along $\langle 100 \rangle$ and $\langle 110 \rangle$ are $4\pi/a$ and $4\sqrt{2}\pi/a$, respectively. Furthermore, the data points are plotted in only half of the first Brillouin zone (say, for Γ to X in the $\langle 100 \rangle$ case) so that the points in the other half of the zone will be mapped over by assuming the bands are symmetric with respect to the Γ point, which is expected to be true from symmetry considerations. In all plots, the nonmagnetic labels have been used. It should also be pointed out that the surface reconstruction of the transition metal monooxides was found to be very small.[47] This increases the credibility of the result of photoemission data from NiO.

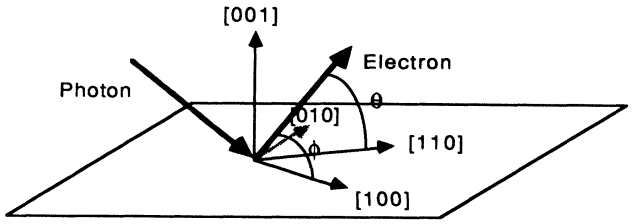

FIG. 1. Experimental geometry for off-normal-emission data along [110]. The definitions of the angles θ and ϕ are illustrated.

III. NORMAL EMISSION FROM THE NiO (100) SURFACE

Figures 2 and 3 present normal emission data from the NiO (100) surface in the photon-energy range of 13–86 eV. The data shown in the two figures were recorded from two samples where the Fermi levels were pinned at slightly different energy positions in the gap. There are five prominent features observed in the experimental data, which we assign as *A*, *B*, *C*, *D*, and *E*, respectively. Feature *B* (in Fig. 3) has been previously interpreted as the d^7 satellite, which is pushed up to higher binding energy due to the strong on-site Coulomb interaction.[16,17] Its intensity at lower photon energies is very weak (it is not observable in Fig. 2), and it gets stronger at higher photon energies. This photoionization cross-section behavior is consistent with its Ni 3*d* nature. Also, its intensity increases dramatically at a photon energy of 68 eV as compared with the 64-eV spectra, indicating a resonance behavior, which is consistent with earlier results.[19,20]

The features *A* (▽) and *C* (△) are believed to be mainly Ni 3*d* derived, and are not very dispersive. On the other hand, one can still see the effects of the translational symmetry on feature *A* in terms of its remarkable intensity modulations. Figures 4 and 5 give details of feature *A* at normal emission. The remarkable change of the line shape as a function of the photon energy suggests that it

has at least three components: A', A'', and A'''. Feature C is also believed to be a mainly Ni $3d$ derived feature, and is basically nondispersive. Therefore, the total energy spread of the Ni $3d$ band is quite sizable (about 2.5 eV), but the data does not indicate strong dispersion of individual bands along this direction.

Features E (●) and D (○) show strong dispersions and intensity modulations as a function of photon energy, which is consistent with the earlier assignment that these are oxygen features.[18] Feature E starts at lowest energy near $h\nu=17-19$ eV, then shifts monotonically towards higher energy until near $h\nu=26$ eV, where its behavior becomes complicated. At photon energies of 27 and 28 eV, it shows some back bending (moves to lower energy), and the back-bending peaks fade very quickly (crosses in the circle). This bending point cannot be a critical point, as will be justified later, and another branch of feature E continues to shift towards higher energy after 26-eV photon energy (as indicated), where it merges with features C and D at photon energies around 30 eV. As the photon energy continues to increase, feature E begins to bend back to higher binding energy. This suggests that a critical point of feature E is reached at about 30 eV. The situation for feature E near photon energies between 40 and 53 eV is complicated. There are two features observed in the experimental data (marked by crosses). It is not clear which one is feature E. For photon energies above 56 eV, the assignment of the feature E is again unambiguous. Feature D is also believed to be an oxygen feature. At low photon energies, it disperses monotonically towards higher energy (lower binding energy) as the photon energy increases (Fig. 2), and then flattens out at higher photon energies (Fig. 3).

Based on the experimental data presented in the Figs. 2–5, we can obtain experimental E vs $\mathbf{k}$ relations for the various bands, and the results are compared with a nonmagnetic band calculation in Fig. 6(a). The absolute energy position of Fig. 6(a) is of no significance. The two sets of experimental data from the two samples have been rigidly slid in absolute energy to give the best position to the calculated bands. We would like to point out that the data points at very low photon energies should be considered with caution since the free-electron final-state approximation is expected to break down there.[42] Howev-

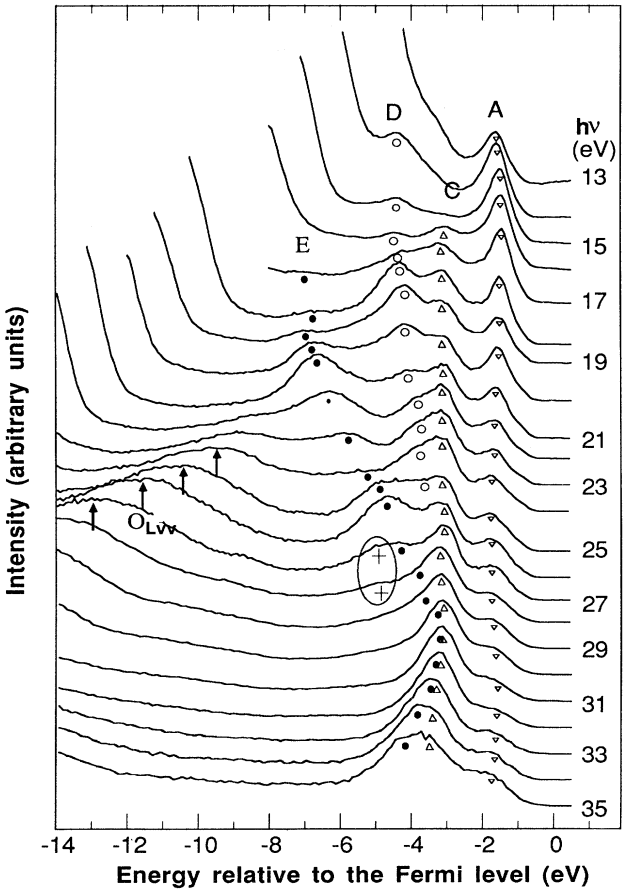

FIG. 2. Normal emission data from NiO ⟨100⟩ in the photon-energy range between 13 and 35 eV. The moving peak marked by the upward arrows is due to emission from the O LVV Auger line. The photon incident angle is 45° with respect to the surface normal.

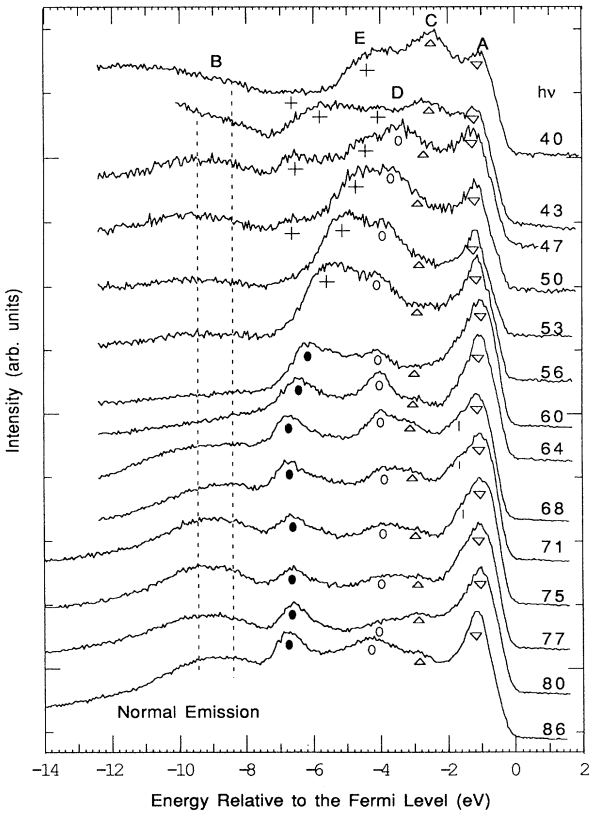

FIG. 3. Normal emission data from NiO ⟨100⟩ in the photon-energy range between 40 and 86 eV. The photon incident angle is 70° with respect to the surface normal.

er, for the vast majority of the data in this figure and all the data to be presented later, this is not a problem.

Several conclusions can be drawn immediately from this figure. In a normal emission experiment, one can only observe the $\Delta 1$ and $\Delta 5$ bands from a fourfold symmetry surface.[48,49] Hence, features E (●) and D (○) correspond to $\Delta 1$ and $\Delta 5$ oxygen bands, respectively, and they are in excellent agreement with the calculated bands. This strongly suggests that our self-consistent local-density-functional band calculation gives a fairly good result for the oxygen bands. This $\Delta 1$ band is significantly (1.6 times) wider than that of an earlier non-self-consistent band calculation.[40]

Despite the good overall agreement between the experimental and calculated nonmagnetic oxygen bands, one can see that the data points denoted by + are not predicted by the nonmagnetic band calculation. To understand these data points, in Fig. 6(b) we compare the experimental data with the results of our antiferromagnetic band calculation. Since our experiments were carried out at room temperature where NiO is in its AF state, this is more reasonable. We may be able to explain some of the + data points by the effect of the antiferromagnetic order. The main effect of the antiferromagnetic order on the oxygen bands is the introduction of flat oxygen bands which are folded in from (π/a) [111] to (π/a) [311], and the splitting of the original $\Delta 1$ band at its crossing point with the flat band. Figure 6(c) illustrates the nonmagnetic bands from [000] to (π/a) [200] and (π/a) [111] to (π/a) [311]. The bands in Fig. 6(b) are a superposition of bands in Fig. 6(c) modified by the magnetic interactions. Those data points which fall within the dashed circle may be interpreted as due to the folded-in bands, and are therefore the effects of the antiferromagnetic order. However, the crossing point of the $\Delta 1$ band and the flat bands in the experimental data seems to be located at higher energy and smaller k value (20% ΓX from the Γ point) than the prediction of the band calculation (30% ΓX from the Γ point). This discrepancy is probably due to the deficiency of the LDA in describing the Ni d

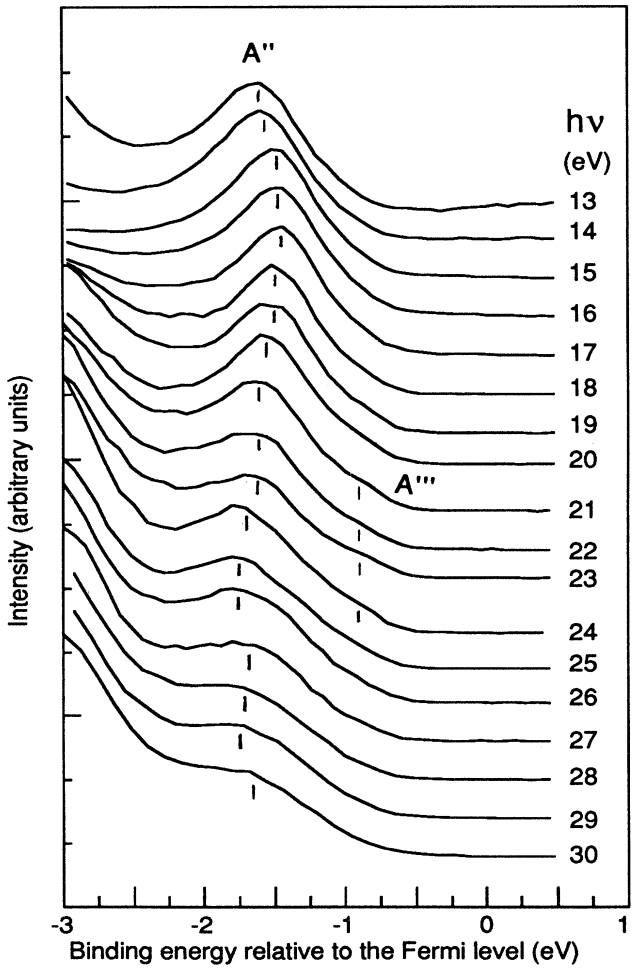

FIG. 4. Details of the Ni 3d band A of Fig. 2. Two components of feature A are visible in the data.

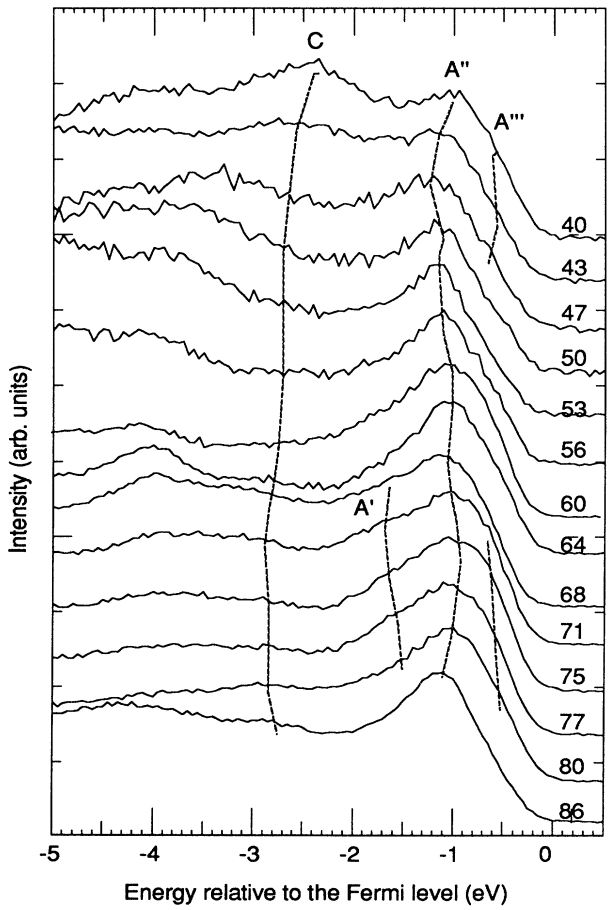

FIG. 5. Details of the Ni 3d bands A and C of Fig. 3. The line shape of feature A changes with the photon energy, indicating it has several components as marked.

bands, which hybridize more strongly with the folded-in p band. If we shift the calculated flat bands upwards, then the experimental and theoretical results will agree quite well. However, even with the consideration of the antiferromganetic order, we still cannot understand the few data points (+) which seem to be randomly distributed. The folded-in theoretical oxygen band was not observed in the normal-emission data near the Γ and the X points. This result is different from the off-normal-emission data to be discussed in the next section.

In contrast to the oxygen bands, we find that the agreement between the experiment and the nonmagnetic Ni $3d$ bands is not as good. Feature A is believed to be due to emission from the Δ1 and Δ5 bands. The observed energy dispersion of feature A along ⟨100⟩ is much smaller than the theoretical prediction. On the other hand, it is interesting to note that the trend of its dispersion is consistent with the theoretical calculation (i.e., the band moves toward higher energy as one goes from the Γ to the X point). The assignment of feature C is somewhat complicated. If we want to stick with the nonmagnetic bands, the only possibility is that it corresponds to the high density of states (in the form of one-dimensional density of states) of the 2′ band at the X point, which is picked up only because of the finite acceptance angle of the electron analyzer.[50] The difficulty associated with this interpretation is that the intensity of feature C is too strong, since the 2′ band is forbidden by the selection rule if we have an infinitely small acceptance angle. This comparison shows poor agreement between our data and the nonmagnetic LDA bands.

The overall agreement between the experiment and the band theory improves dramatically if we consider the antiferromagnetic order which makes the theoretical bands

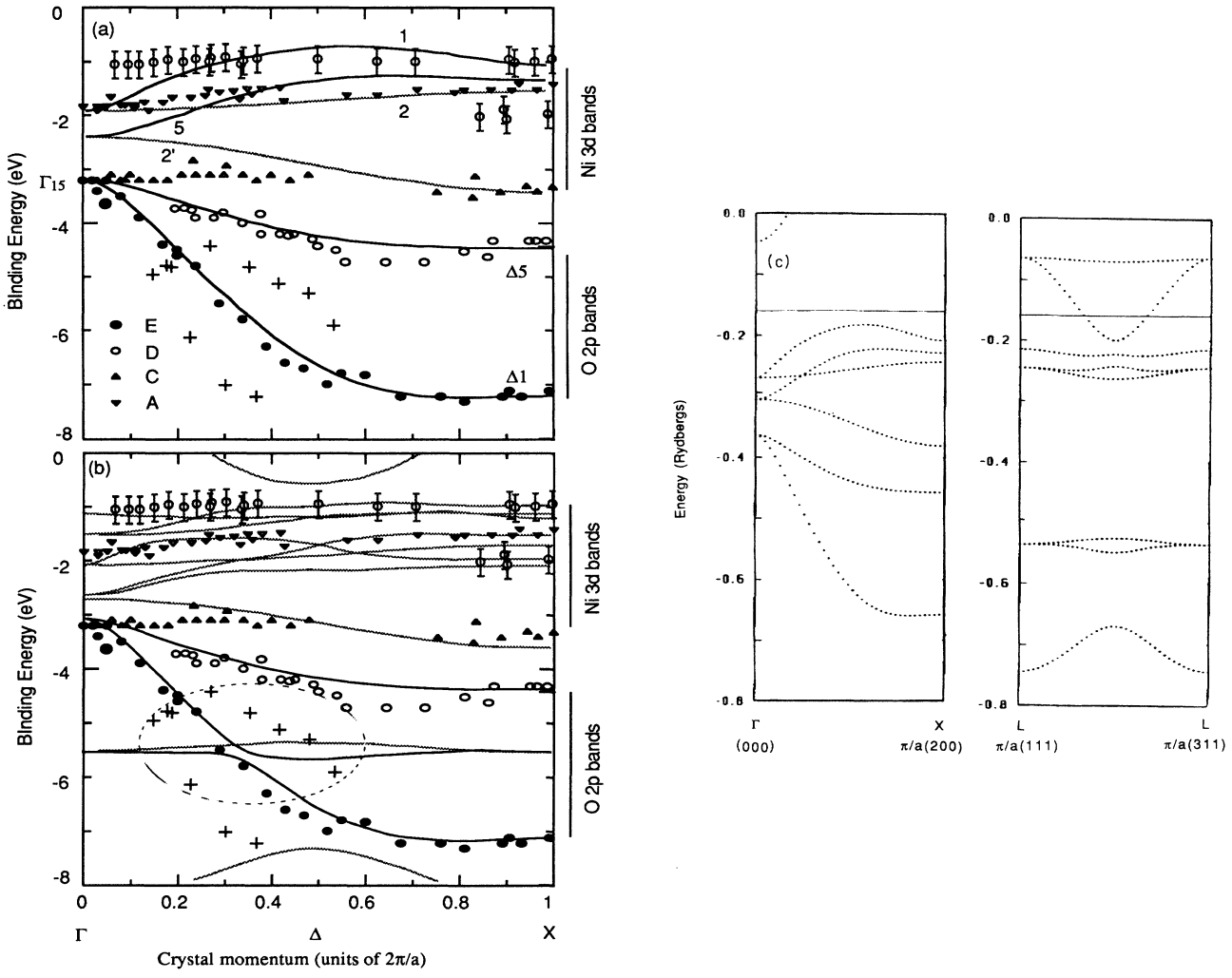

FIG. 6. (a) Comparison of the experimental E vs $\mathbf{k}$ relations with a nonmagnetic band calculation. The absolute energies of the two data sets from different cleaves are adjusted to give the best comparison of the calculation. (b) Comparison of the experimental data with an antiferromagnetic band calculation. In the upper panel, the bands which are forbidden by selection rules in the normal emission is marked by gray lines. In the lower panel, all but the two of the oxygen bands (corresponding to the nonmagnetic case) are marked by gray lines. (c) Nonmagnetic bands from [000] to (π/a) [200] and (π/a) [111] to (π/a) [311].

flatter. A detailed comparison of various components of feature A with the antiferromagnetic band calculation is difficult, since the calculated bands are very complicated (a very large number of bands are located in a small energy range). However, the experimental data seem to fall on top of the theoretical results. There is also a flatter magnetic band near feature C, which, in the framework of the band theory, corresponds to feature C. This band provides an opportunity for us to compare the data with the theory, since it is well separated from the other bands. Generally speaking, both the data and the antiferromagnetic band calculation show that the overall spread of the Ni $3d$ band is quite sizable (~ 2.5 eV), but the energy dispersion of the individual bands is difficult to pin down. Another interesting observation is that even though it is predicted by the band theory, the antiferromagnetic band at -8 eV and the one just below E_F (both are only partially shown) are not observed in our data. The absence of the magnetic oxygen band at -8 eV may not be very significant, since the AF effects on the deep lying oxygen bands may be very weak, so that the AF oxygen bands at -8 eV may be hardly visible. The absence of the Ni $3d$ band just below E_F is related to the problem of the insulating gap. In the theoretical calculation, the band just below E_F is empty by counting electrons (i.e., it is above the theoretical Fermi level). Obviously, the data show its predicted energy position is wrong, so that it is below the experimentally determined Fermi level. This problem of the insulating gap has long been recognized to be a major difficulty for the band theory.

IV. OFF-NORMAL-EMISSION DATA ALONG ⟨100⟩

Figures 7 and 8 present angle-resolved-photoemission data along the NiO ⟨100⟩ direction with photon incident angles of 30° and 70°, respectively. The photon energy and the detection angle are chosen such that $\mathbf{k}_\perp$ is fixed [approximately at $2\Gamma KX(4\pi/a)$], while $k_\parallel$ is varied from the Γ point to the X point along the ⟨100⟩ direction (-8 eV inner potential and $0.95m_e$ effective mass were used to calculate the emission angle and the photon energy). The two data sets presented in Figs. 7 and 8 were obtained from the same crystal cleaved at different times. We can see that the Fermi level was pinned at different positions

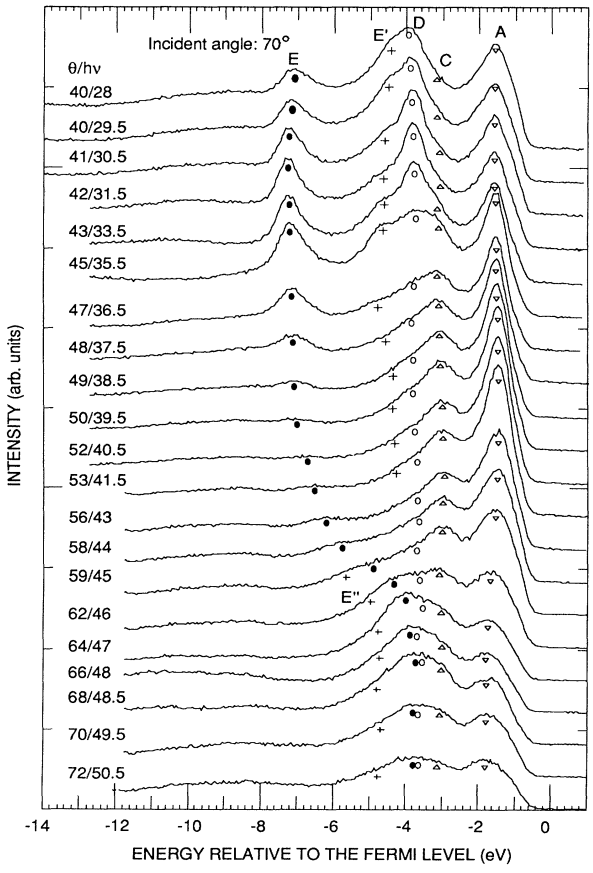

FIG. 7. Stacks of experimental EDC's along NiO ⟨100⟩ with a 70° photon incident angle. The numbers marked on each spectrum are the photon energies and emission angles with respect to the [100] axis in the (100) surface.

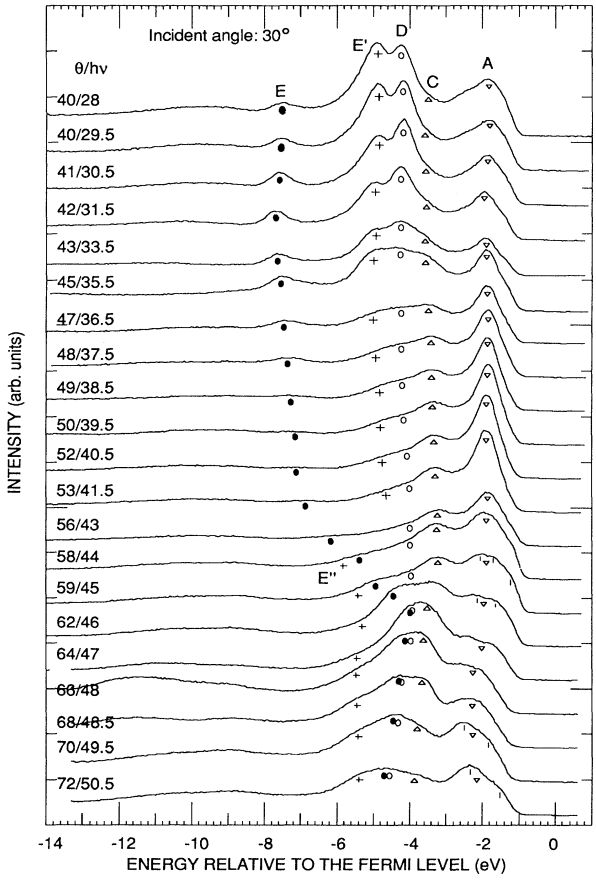

FIG. 8. Stacks of experimental EDC's along NiO ⟨100⟩ with a 30° photon incident angle. The numbers marked on each spectrum are the photon energies and emission angles with respect to the [100] axis in the (100) surface.

in the energy gap. However, this will not affect our analysis of the experimental data.

There are striking similarities between the off-normal-emission data in Figs. 7 and 8 and the normal emission data presented in Figs. 2 and 3. The lowest oxygen feature, E (●), is very dispersive, just like its counterpart in the normal emission data. From the upper spectrum to the lower spectrum (which corresponds to going from X to Γ in k space), feature E moves continuously towards higher energy (lower binding energy) in almost exactly the same way as in the normal emission data. Above the $h\nu/\theta$ value of 59/45, the assignment of feature E becomes more complicated. A new branch is split off to form a new band E'' (denoted +), which we assign to the antiferromagnetic bands (see discussion later). For the bands with intermediate energy (−3 to −5 eV), there are differences between the off-normal-emission data and the normal-emission data. Instead of just two features (C and D) in the normal-emission data, there are three features, C, D, and E', in the off-normal-emission data. This is seen most clearly in the spectra at low photon energies and emission angles (e.g., $h\nu/\theta=45/35.5$). The features with higher energies (lower binding energy) are believed to be related to features C (△) and D (○) in the normal emission data, and the extra feature E' (+) is believed to be due to the AF order (see discussion later). The features A (▽) and C (△) are Ni $3d$ bands. They show stronger intensity modulations in the off-normal-emission data than in the normal-emission data.

Figures 9 and 10 give details of features A and C from Figs. 7 and 8, respectively. The experimental curves from the top to the bottom correspond to the crystal momentum value from near 0 (Γ point) to near $2\pi/a$ (X point). From these data alone, it is difficult to judge whether the remarkable line-shape changes are due to energy dispersion or intensity modulation. Four of the spectra from Fig. 10 are chosen to be blown up to give a better view of the data points (as shown in Fig. 11). Thus we see that the statistics of the data is good enough to reveal the details of feature A. In agreement with the normal emission data, the Ni $3d$ band feature A consists of at least three components denoted by A', A'', and A'''. This can be most clearly seen in the blown-up spectrum of 59/45 in Fig. 11. We find that the features are much broader than our instrumental energy resolution (0.15 eV), which reflects that the intrinsic width of the various components of the feature A is quite large. This could be due to either the lifetime broadening or the fact that each component has several bands involved (as suggested by the antiferromagnetic band calculation). Unlike feature

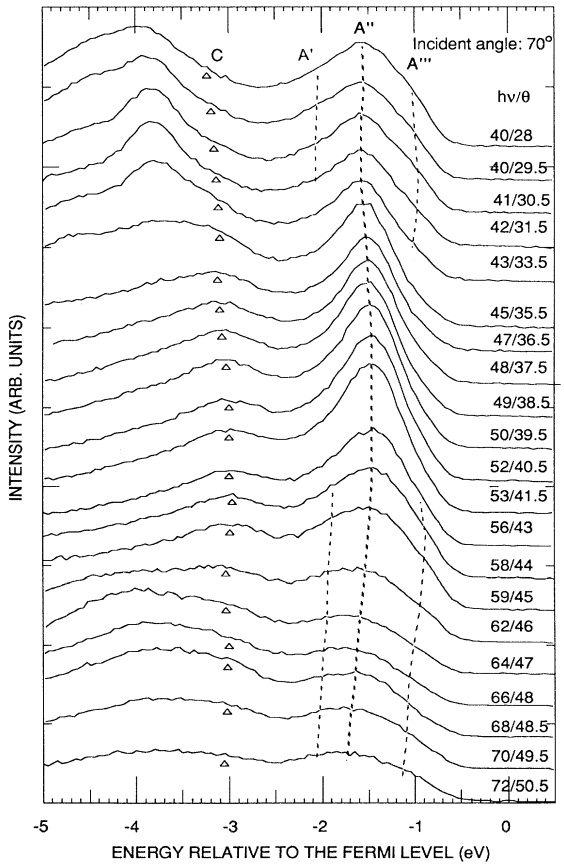

FIG. 9. Details of features A and C of Fig. 7.

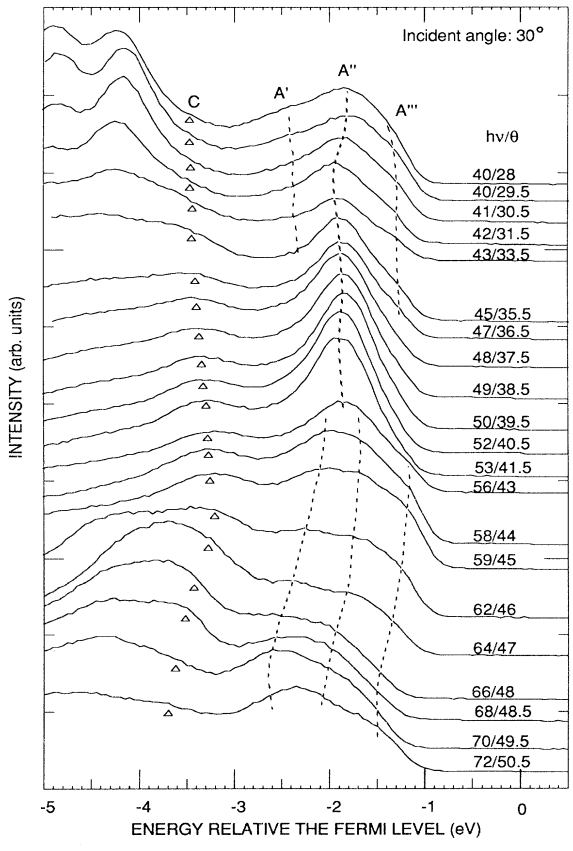

FIG. 10. Details of features A and C of Fig. 8.

A, feature C seems to have only one component. This shows that most of the $3d$ bands are in the energy range of feature A, a reason why feature A is stronger in the angle-integrated XPS data (where only the Ni $3d$ states are detected).[51]

Comparing the data of Figs. 7–11, we can also see the strong effects of the photon polarization. For materials with fourfold symmetry, it is established that only states with $\Delta 1$ and $\Delta 5$ symmetries are observable in the normal emission experiments.[48,49] The states with $\Delta 1$ symmetry will be observed if the polarization of the light is normal to the crystal surface, while the states with $\Delta 5$ symmetry will be observed if the polarization of light lies in the crystal surface. In the case of off-normal-emission experiments, no such rigorous selection rules exist. However, we can still obtain some information about the symmetry of the states by varying the photon polarization. With the same emission angle, the emission intensity of states with $\Delta 1$ ($\Delta 5$) symmetry is stronger with the photon polarization perpendicular (parallel) to the surface. Feature E (●) is much stronger in the 70° incident-angle data as compared with the 30° incident-angle data, suggesting an off-surface symmetry ($\Delta 1$) for it. On the contrary, feature E' (+) is stronger in the 30°-incident-angle data as compared to the 70°-incident-angle data. Similarly, feature A'' is stronger in the 70°-incident-angle spectra relative to features A' and A''', indicating it has off-surface symmetry or the others have the in-surface symmetry.

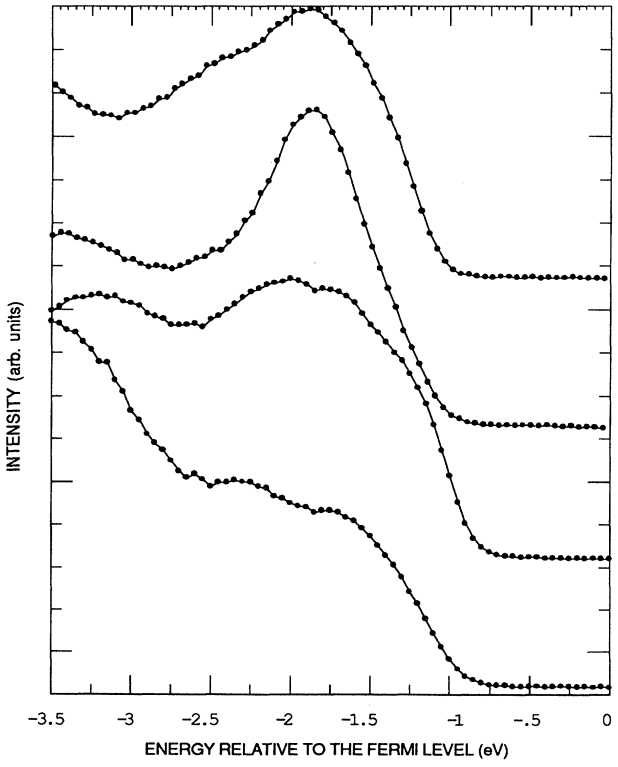

FIG. 11. Selected spectra from Fig. 8 to demonstrate that at least three components of feature A were resolved.

From these data, we were able to obtain experimental E vs $\mathbf{k}$ relations. Figures 12 and 13 present the experimental E vs $\mathbf{k}$ relations together with band calculations for data obtained with the photon incident angles of 70° and 30°, respectively. In Fig 12, the experimental data is compared with both the nonmagnetic as well as the antiferromagnetic LDA calculations. When the data is compared with the nonmagnetic bands in the upper panel, we can see that the experimental E band (●) agrees with the $\Delta 1$ band very well except for a few points near Γ. The experimental $3d$ bands are very flat, but their relative en-

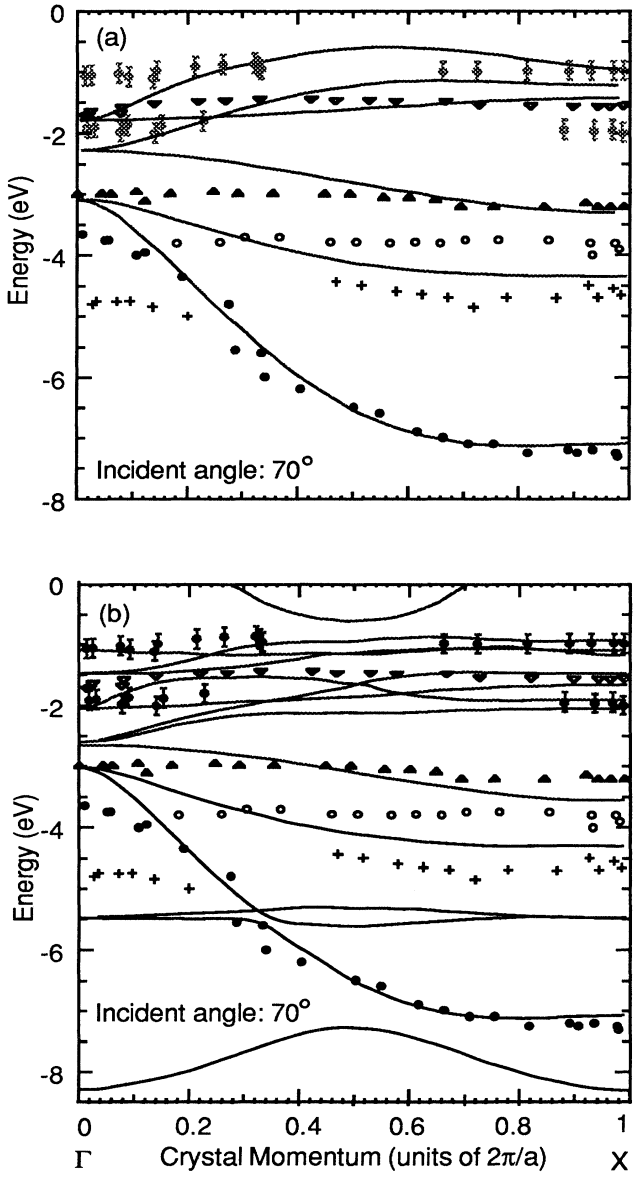

FIG. 12. E vs $\mathbf{k}$ relation from data in Figs. 7 and 9 in comparison with (a) the nonmagnetic and (b) the antiferromagnetic LDA band calculations.

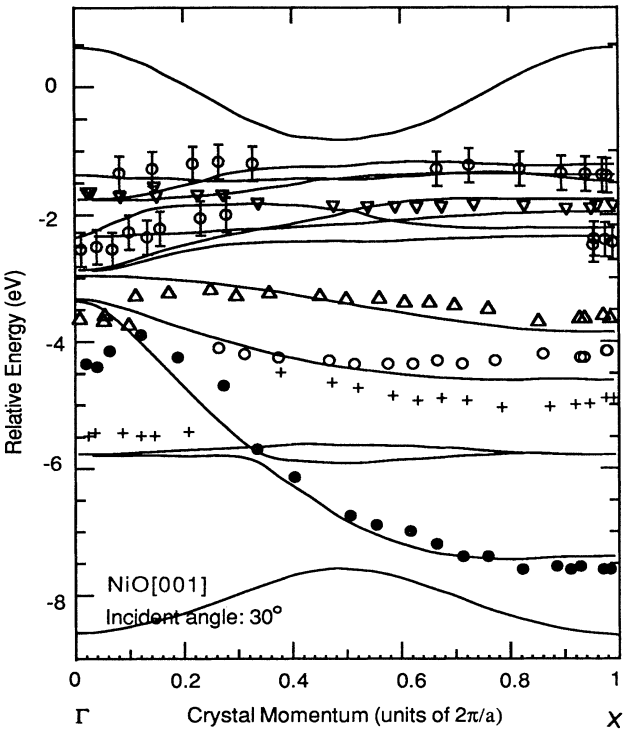

FIG. 13. E vs $\mathbf{k}$ relation from data in Figs. 8 and 10 in comparison with the antiferromagnetic band calculation.

ergy positions fit the calculation quite well. However, in the energy range between -2 and -5 eV, agreement between the experiment and the nonmagnetic band is poor. There are three experimental bands observed, in contrast to only two theoretical bands.

Now we turn to the comparison between the experimental data and the antiferromagnetic band calculations. Immediately, we can see that the agreement between the experiment and the theory is improved by considering the antiferromagnetic order: (a) The AF order makes the $3d$ bands flatter and thus improves the agreement between the experiment and the theory. (b) With the inclusion of the AF order, we can at least understand the reasons why there are extra bands like E' (+) and E'' (+). They are probably related to the flat band crossing the $\Delta 1$ oxygen band near -5.5 eV, which is folded back from (π/a) [1,1,1] to (π/a) [3,1,1] as a result of the antiferromagnetic order along the [111] direction. The fact that the measured band lies higher than the calculated band indicates that the LDA calculation overestimates the p-d hybridization energy (as a result, the flat band is pushed too low by the band calculation since it has more $3d$ character). From these data we can also see that the effect of the antiferromagnetic order on the oxygen bands is more visible in the off-normal-emission data than in the normal-emission data. In the normal-emission data, the folded-in oxygen band is not observed near the Γ and the X points.

As shown in Fig. 12(b), it is interesting to note that the experimental data points fall on top of the calculated bands. The energy separation between the $3d$ and $2p$ bands from the experimental data is in good agreement with the calculated result. This is very different from the earlier result that one has to shift the calculated $3d$ spectral weight by about 2 eV to fit the angle-integrated experimental data.[52] It appears that the incorrect conclusion was drawn by misinterpreting the angle-integrated photoemission data. Since the angle-resolved-photoemission data provide much more detailed information about the band structure than the earlier angle-integrated photoemission data, we feel very confident about the new result. Furthermore, the fact that we can see several components in feature A but only one component in feature C is also in agreement with the calculated result that there are more bands in the energy range of the feature A.

Feature E (●) agrees with the calculated $\Delta 1$ band almost perfectly except for the points near Γ, indicating that the LDA calculation describes the oxygen band very well. The disagreement between the experimental and theoretical E band near the Γ point is different from the normal emission data where the agreement between the two is very good. Even though it is difficult to be absolutely sure about all the reasons behind this, the following experimental difficulty is certainly a contributing factor: During the off-normal-emission measurements, we hoped to fix $\mathbf{k}_\perp$ to the Γ ($\mathbf{k}_\perp = 2n\Gamma KX$) point. In reality, however, this is very difficult to achieve with high precision because of various experimental constraints. For example, there are several peaks in each spectrum with different kinetic energies (they could differ in kinetic energy by about 6–7 eV), it is then impossible to choose a set of photon energy and emission angle that will fix $\mathbf{k}_\perp$ of all the peaks (corresponding to different bands) at the Γ point. Therefore, $\mathbf{k}_\perp$ could deviate from the Γ point by as much as 10%. Thus, in the E vs $\mathbf{k}_\parallel$ figure we have here, the $\mathbf{k}_\parallel = 0$ point might not coincide exactly with the Γ point of the band theory. Since the band energy (of the $\Delta 1$ band, in this case) changes with the uncertainty of $\mathbf{k}_\perp$ most sensitively near the Γ point, it is very reasonable that the problem is most severe there. In the normal-emission experiment, it is much easier to make sure that $\mathbf{k}_\parallel = 0$, then the Γ point will be reached when $\mathbf{k}_\perp = 0$. In this sense, the normal-emission data is more reliable. In addition, due to the proximity of the other bands to the E band at the Γ point, the error bar of the energy position of this band becomes larger.

We believe feature D (○) is the $\Delta 5$ oxygen band which appears to lie higher in energy than the calculation. This result is somewhat different from the normal-emission result of Fig. 6 and the error in $\mathbf{k}_\perp$ could again be a problem. Feature C (△) is believed to be related to the lowest Ni $3d$ band, which is well separated from the other $3d$ bands so that it is the best candidate to compare with the theory. If this is correct, then the experimental $3d$ band is clearly narrower.

As we have discussed earlier, feature A (▽), which consists of three components, represents the main part of the $3d$ bands, where many bands are squeezed together in a very narrow energy range. The error bar for the data points of A' and A'' components is used to indicate the

fact that their energy positions are hard to determine with high accuracy. A rigorous comparison between theory and experiment for the main $3d$ band is very difficult because the calculated bands are too complicated in a narrow energy range. We notice that the resolving power here is limited by the lifetime broadening (or the intrinsic width) of the Ni $3d$ bands so that an improved energy resolution would not help us in resolving the various $3d$ bands.

Figure 13 shows the experimental E vs $\mathbf{k}$ relation for the NiO (100) surface with an incident photon polarization of 30°. We note the overall similarity between this data set and that in Fig. 12. This is very encouraging, since it shows that the experimental results are very reproducible from various measurements with different experimental geometries. However, minor differences do exist. First let us look at the Ni $3d$ bands in the region of feature A (noted by ∇ and the points with error bars). We find that this data set agrees with the LDA bands better than the data set in Fig. 12. This is particularly true for the lowest A''' feature near the Γ point. As one moves from the Γ point to the X point, the experimental A''' band disperses upward, which is consistent with the calculated bands there. Since feature A''' is stronger in this set of data, its energy position can be better determined. In this sense, we believe that this data set is more reliable than that in Fig. 12, even though the differences are marginal. For the C ($\triangle$) band, the result in this set is basically the same as that in Fig. 12. The experimental data points and the LDA $3d$ bands are at similar energy positions. However, the experimental band is narrower than the theory.

Now let us look at the oxygen bands. For $\mathbf{k}$ values smaller than $0.2\Gamma X$, the E' (+) band is located at lower energy than its counterpart in Fig. 12. Interestingly, this makes this fraction of the data agree with the band calculation better than in Fig. 12. The experimental points, however, still lie at higher energy than the calculated flat band energy. For the k values larger than $0.4\Gamma X$, the results for the E' (+) bands in Figs. 12 and 13 are very similar. Then the problem in Fig. 13 is that the E' band, which according to the band calculation should be very flat, differs in its energy by about 0.5 eV on left and right sides of the E (●) band, which it should cross. To make the situation even worse, the trend of the dispersion of this band E (+) is such that its branches on the left and the right side of the E (●) band are not moving in the direction so that they will meet with each other at the crossing point with the E band, as the band theory is telling us. In fact, the trends of the dispersions of the two branches are going the opposite way, so that they will not meet with each other. We do not know what the reason behind this result is. Certainly this E' band does not agree with the LDA calculation. The difference in the two sets of data is most likely caused by the uncertainties in determining the energy of the E' and E'' band. Because the polarizations of the incoming photons are different in the cases, the relative intensity of the feature E' (see Figs. 7 and 8) changes dramatically. This leads to the result in which the band appears to be located at different energy positions, a major source of uncertainties of the peak position in our case. Of course, we cannot rule out the possibility that the E' bands in the two data sets are actually due to two different bands.

An important disagreement between the experimental result and the magnetic band calculation is that some of the magnetic bands have never been observed in the experiment. Specifically, the oxygen band near -8 eV and the Ni $3d$ band just below E_F are not observed in the experimental data. Since we have taken the same data with three very different geometries, it is impossible that the emission will be completely banned in all cases by selection rules. There must be other reasons why these bands are not present. The absence of the oxygen band near -8 eV may be explainable by the fact that magnetic effects on the oxygen bands are weaker, since the magnetic moments are located within the cation sites. The absence of the Ni $3d$ antiferromagnetic band between E_F and the first observed band (typically at -1 eV) is related to the problem of the insulating gap, as we have pointed out at the end of Sec. III.

As we have seen above, even though the details from the different data sets may vary, the overall consistency of the experimental data from both normal emission and off-normal emission is overwhelming. The fact that we can get almost the same conclusions from different sets of experimental data (including both normal-emission and off-normal-emission experiments) makes us very confident with our interpretation and the parameters we used.

V. OFF-NORMAL EMISSION ALONG THE ⟨110⟩ DIRECTION

Figure 14 presents a set of angle-resolved-photoemission data from a cleaved NiO (100) surface. The photon energies and the emission angles are so chosen that $\mathbf{k}_\perp$ is fixed at ΓKX, while $\mathbf{k}_\parallel$ is changed along the ⟨110⟩ direction. Like the results from the ⟨100⟩ direction, five prominent features are observed in the experimental data. These features are denoted as $A1$, $B1$, $C1$, $D1$, and $E1$, respectively. Feature $B1$ is the NiO satellite caused by the strong on-site Coulomb interactions among Ni $3d$ electrons (actually it has two components). Features $E1$ (●) and $D1$ (○) are oxygen features, and they show clear energy dispersions. There are also two weak features in the same energy range, which are denoted by $E1'$ (+) and $E1''$ (×). Features $A1$ (∇) and $C1$ ($\triangle$) are believed to be Ni $3d$ bands, and are basically nondispersive. However, the effects of the translational symmetry can still be clearly seen in these features. The details of the features $A1$ and $C1$ are presented in Fig. 15. The feature $A1$ clearly has several components while feature $C1$ only has one component, which is very similar to that of A and C.

The experimental E vs $\mathbf{k}$ relations obtained from data in Figs. 14 and 15 plotted in Fig. 16 together with the results of a nonmagnetic band calculation along ⟨110⟩. The absolute position of the energy is arbitrarily aligned to give the best comparison between the experiment and the theory. Feature $E1$ (●) is apparently the Σ_3 oxygen

band. One can see that the experiment and the theory agree reasonably well except for the data points near Γ. As in the off-normal-emission data from ⟨100⟩, the disagreement between the experiment and the theory near the Γ point is most likely due to the uncertainties in $\mathbf{k}_\perp$. The fact that the peak positions in the experimental data are difficult to be determined unambiguously also contributes to the error here. The origin of the feature $E1'$ (+) is not yet clear and will be discussed later. The feature $E1''$ (×) could be related to the oxygen Σ_1 band, which also agrees with the calculation nicely. The feature $D1$ (○) is most likely the Σ_4 band; its downward trend of dispersion from the X point to lower k value agrees with the calculated result reasonably well. Good agreement is also found for its energy position near the X point. However, compared with the theoretical band, the experimental band appears at a too-high energy position. From the above discussion, we can see that the overall agreement between the experimental and the theoretical results for the Σ_3 and Σ_4 oxygen bands is quite good. This is very consistent with the earlier finding from NiO ⟨100⟩ that the agreement between the experimental and band theoretical result of the Δ1 and Δ5 oxygen bands is very good.

For the Ni 3*d* bands along ⟨110⟩, on the other hand, we can see that the agreement between the experiment and the nonmagnetic band theory is rather poor. The experimental 3*d* bands $A1$ (▽) and $C1$ (△) are basically nondispersive. The theoretical 3*d* bands, on the other hand, consist of both less-dispersive and dispersive ones. The less-dispersive 3*d* bands are located at approximately the same energy positions as the feature $A1$ (▽). The energy position of the $A1'$ and $A1'''$ components are also indicated in the data with some symbolic error bars. However, the very dispersive 3*d* bands do not find their experimental counterparts at all. Several reasons may explain why they were not observed experimentally. The first is that they are made invisible by some selection rules. Since we are doing off-normal-emission experiments, we cannot see a good reason why they should be completely banned by selection rules so that this is not very likely. The second reason is that antiferromagnetic order makes the 3*d* bands narrower. As we will see in the next paragraph, this can partially account for the ob-

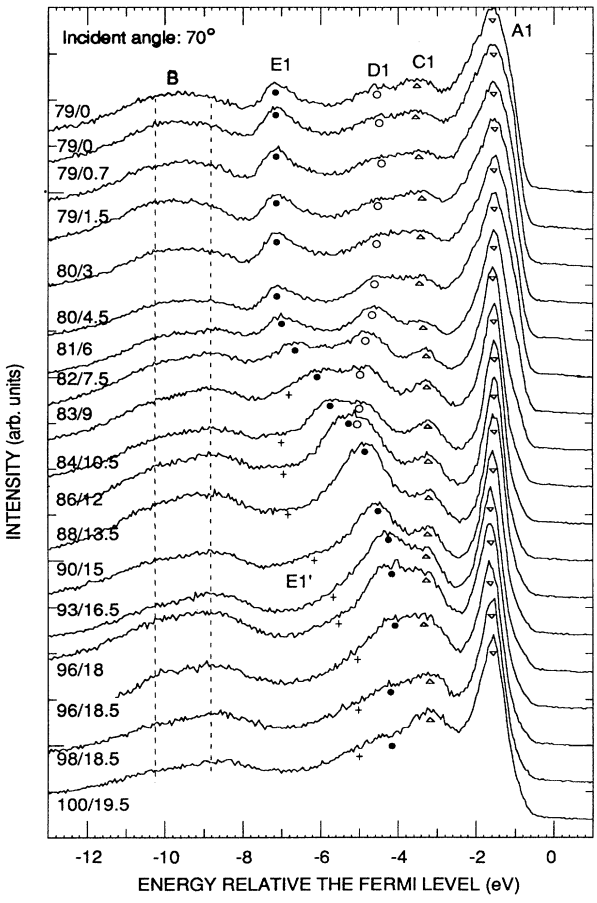

FIG. 14. Stacks of the experimental data along ⟨110⟩ with a photon incident angle of 70°. The numbers marked on each spectrum are the photon energies and angles one has to change with respect to the two perpendicular ⟨100⟩ axes in the (100) surface in order to vary $\mathbf{k}_\parallel$ along the ⟨110⟩ direction in the (100) surface.

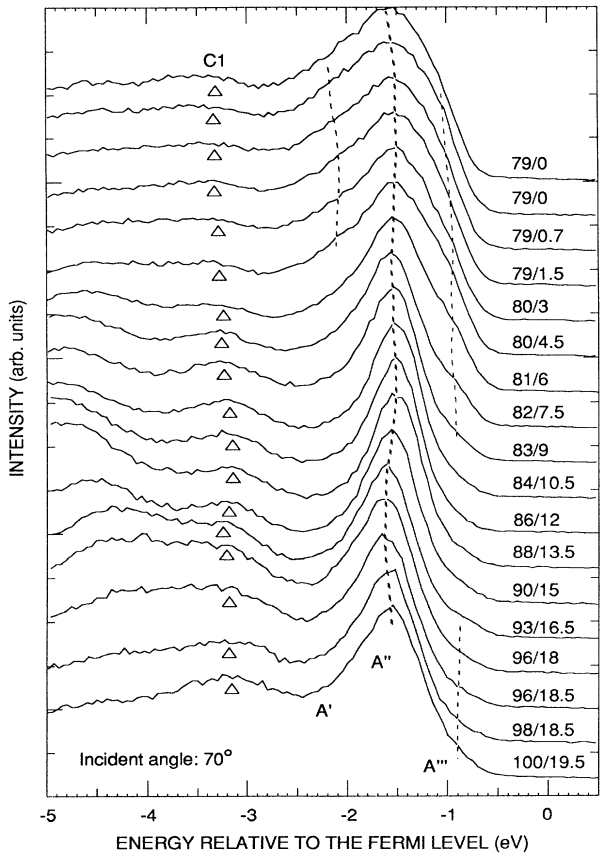

FIG. 15. Details of features *A* and *C* in Fig. 14.

served difference between the experiment and the theory. The third reason is related to the problem for the band theory to reproduce the experimental insulating gap. The topmost dispersive $3d$ band along this direction cuts the Fermi level, which incorrectly give the metallic ground state of NiO. On the other hand, feature $C1$ cannot find its theoretical correspondent, which is very similar to feature C in the $\langle 100 \rangle$ data.

Because NiO was in its antiferromagnetic state at room temperature when the data were recorded, one should compare our data with the results of antiferromagnetic band calculations. Since the AF order of NiO is along the [111] direction, there are two inequivalent $\langle 110 \rangle$ directions, which cannot be distinguished by techniques like x-ray diffraction. The comparisons between the experimental data and the band calculations are presented in Figs. 17 and 18. Generally speaking, the experimental data do not distinguish one direction from another. It is likely that the crystal contains many domains with different magnetizations. Hence what we observed is probably a superposition of the two directions. In principle, we should compare the data with the extrapolation of the theory from the two directions. However, since the level of agreement (or disagreement) between the experiment and the theory along the two directions is very similar, such an extrapolation is not critical for our discussion. The overall agreement between the experimental data and the band calculation is improved by considering the antiferromagnetic order. This is the same conclusion we draw from the experimental data along $\langle 100 \rangle$. First of all, the theoretical Ni $3d$ bands become narrower, which significantly improves the agreement between the experiment and the theory. The experimental $A1$ band (with several components as noted by the ∇ symbol and points with error bar) lies on top of the most densely populated Ni $3d$ bands with a few exceptions at the Γ point. We can regard the feature $E1'$ (+) as due to an antiferromagnetically back-folded band near -4.7 eV. From the above discussion, we conclude that it is important to include the antiferromagnetic order in order to interpret the experimental data. However, the effects due to the antiferromagnetic order do not show up very strongly in the experimental oxygen data. For example, we do not see in our data a strong feature corresponding to the antiferromagnetically back-folded band at -8 eV.

Figures 19 and 20 show two additional sets of angle-resolved-photoemission data along NiO $\langle 110 \rangle$ with different photon incident polarizations. We assign the

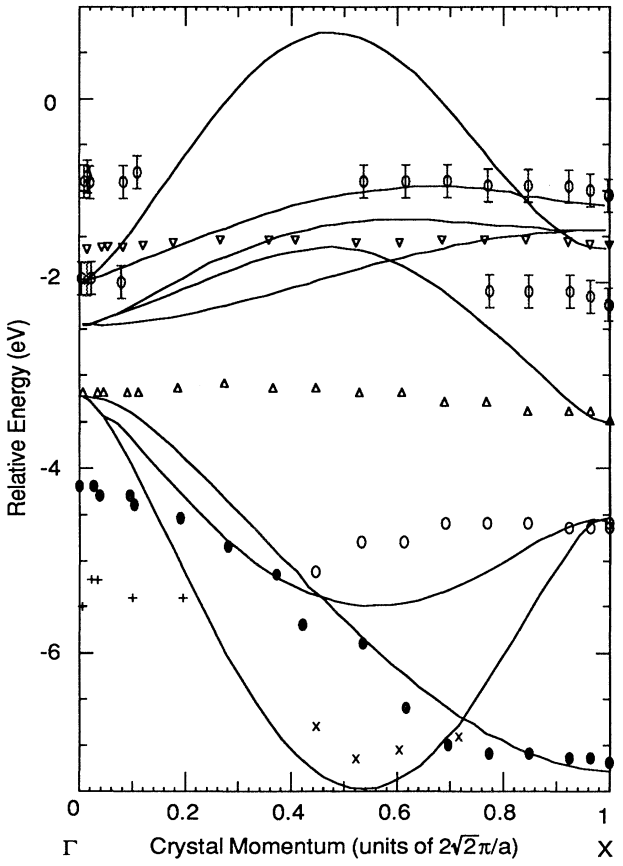

FIG. 16. Comparison of experimental E vs $\mathbf{k}$ relations from data in Figs. 14 and 15 with nonmagnetic bands along the $\langle 110 \rangle$ direction.

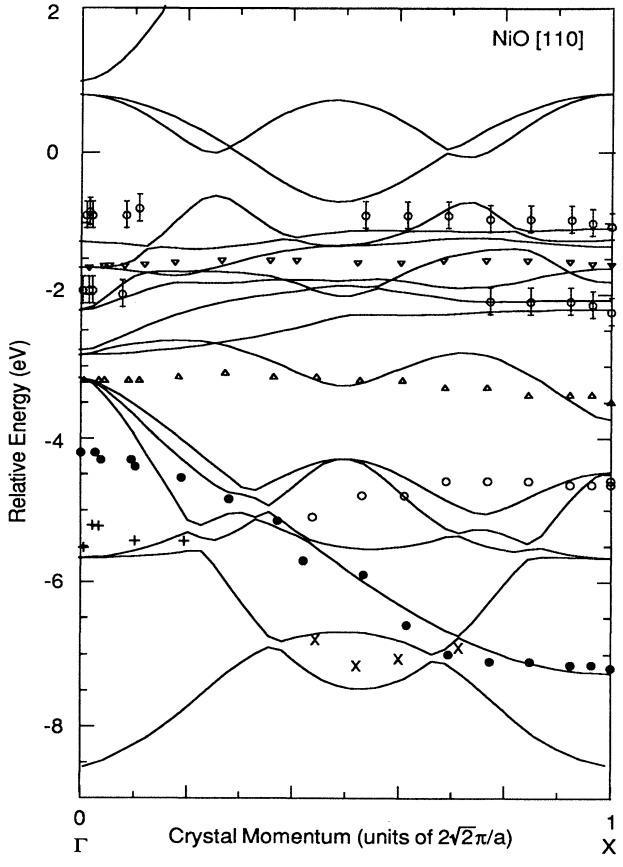

FIG. 17. Comparison of experimental E vs $\mathbf{k}$ relations from data in Figs. 14 and 15 with the antiferromagnetic bands along [110].

five experimentally observed features to $A1$, $B1$, $C1$, $D1$, and $E1$. Again, feature $B1$ is the valence-band satellite which shows its resonance at the 68.5/48 spectra. Features $A1$ and $C1$ and Ni $3d$ bands, while features $D1$ and $E1$ are oxygen $2p$ bands. The individual oxygen bands are somewhat difficult to follow in these data; therefore, the features are denoted by the same symbol (●). We notice that the effects of the difference in photon polarization on the photoemission spectra is significantly weaker than those along ⟨100⟩ (see data in Figs. 7 and 8).

Following the standard procedure, we obtain the experimental E vs $\mathbf{k}$ relations which are shown in Figs. 21 and 22. The experimental data were compared with the antiferromagnetic bands along [110]. The results from these two data sets are consistent with the general picture we get so far. The LDA calculation gives essentially the correct energy positions of various bands. For the oxygen bands, the general trends of dispersion seen in the data are consistent with the calculated results, even though it is difficult to follow each individual band in these two sets of data. There are many flat $3d$ bands in the energy region of feature $A1$, which is probably why its relative intensity is always strong in the experimental

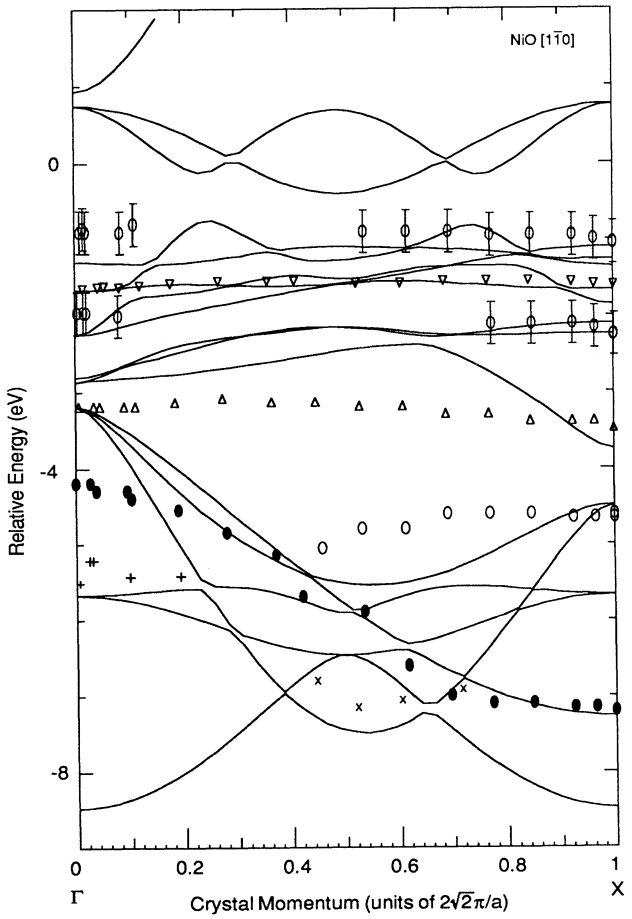

FIG. 18. Comparison of experimental E vs $\mathbf{k}$ relations with the antiferromagnetic bands along [1$\bar{1}$0].

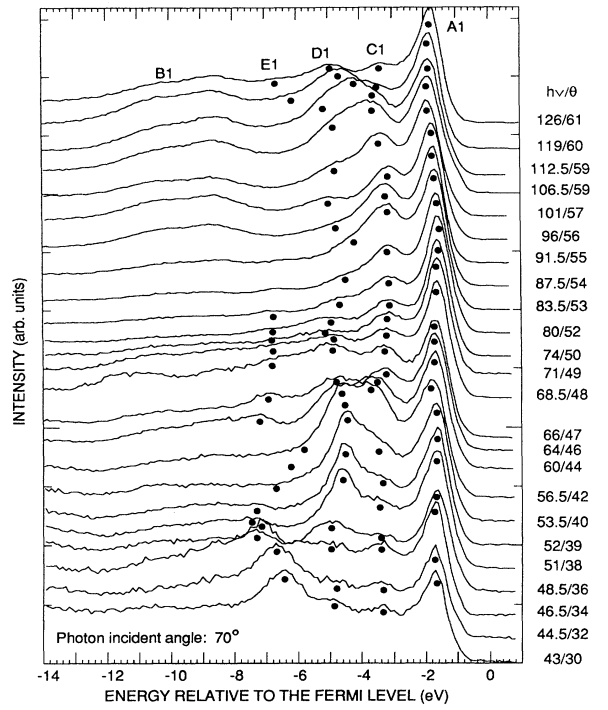

FIG. 19. Angle-resolved-photoemission data of NiO ⟨110⟩ direction with the photon incident angle of 70°.

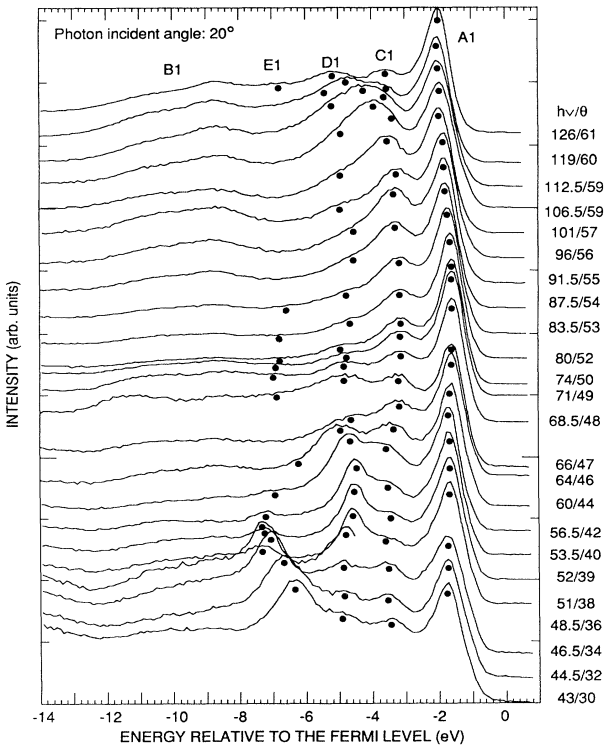

FIG. 20. Angle-resolved-photoemission data of NiO ⟨110⟩ direction with the photon incident angle of 20°, except for the lowest six curves which have a photon incident angle of 40°.

data. In other words, feature $A1$ may consist of several components. The data do not distinguish between the two inequivalent $\langle 110 \rangle$ directions. The same general conclusions hold if we compare the data with $[1\bar{1}0]$.

An important common discrepancy between experiment and theory in Figs. 16–18, 21, and 22 is that while nothing is observed between E_F and -1 eV, the theory always predict some very dispersive bands in this energy range. Since E_F here is the experimentally determined Fermi-level pinning position, and no obvious selection rules prevent us from observing these bands, we should in principle be able to see all the bands below E_F. Again, this is a problem related to the insulating gap. Another important discrepancy between the data and the band calculations is the existence of the infamous valence-band satellite, which will be discussed in detail in the next section.

VI. PHOTON ENERGY AND EMISSION-ANGLE DEPENDENCE OF VALENCE-BAND SATELLITE

As we have pointed out in the Introduction, an important signature of the correlated nature of the late transition-metal compounds is the valence-band satellite. This satellite, which cannot be reproduced by the one-electron theory, is widely believed to be caused by the large on-site Coulomb interaction. In this section, we give details about the observed photon energy and emission-angle dependence of the satellite, which is most likely to be caused by the energy dispersion. To the best of our knowledge, the issue of the satellite energy dispersion has never been addressed experimentally before, even though it has been discussed theoretically.[53,54]

The NiO satellite manifests itself differently in various sets of angle-resolved-photoemission data. It is basically invisible in the low-photon-energy $\langle 100 \rangle$ normal emission data (Fig. 2) but is clearly visible in the higher-photon-energy $\langle 100 \rangle$ normal emission data (Fig. 3). It is quite weak in the off-normal-emission data along $\langle 100 \rangle$ (Figs. 7 and 8), but relatively stronger in the off-normal-emission data along $\langle 110 \rangle$ (Figs. 14, 19, and 20). Figure 23 presents magnified spectra of the satellite region along $\langle 100 \rangle$ with the photon incident angle of 30° (Fig. 8) and 70° (Fig. 7), respectively. Figure 24 gives the spectra of the satellite along the $\langle 110 \rangle$ direction with the photon incident angle of 70° (Fig. 16). Different sets of data were taken from different cleaves of the crystal so that the Fermi level was pinned at slightly different positions. How-

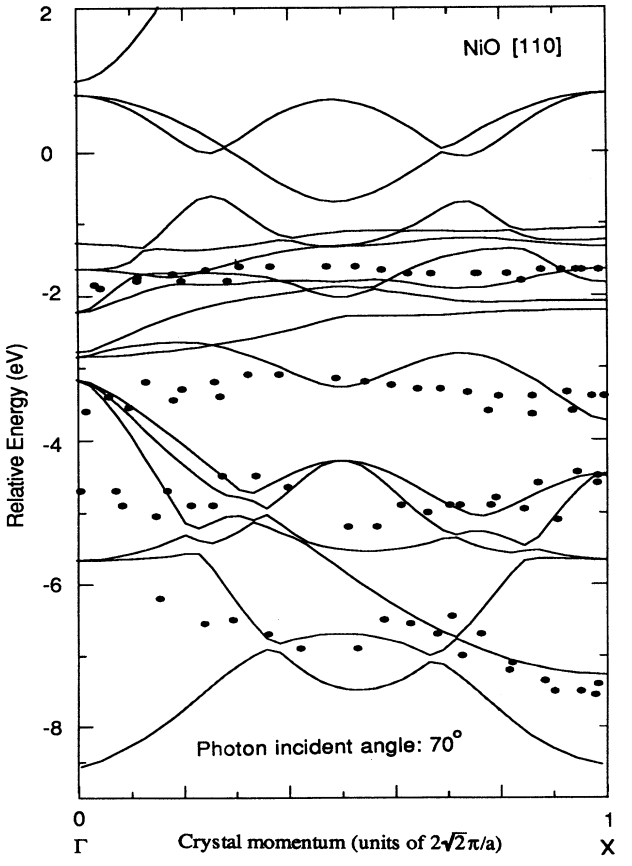

FIG. 21. Experimental E vs $\mathbf{k}$ relation from data in Fig. 19 in comparison with bands along [110].

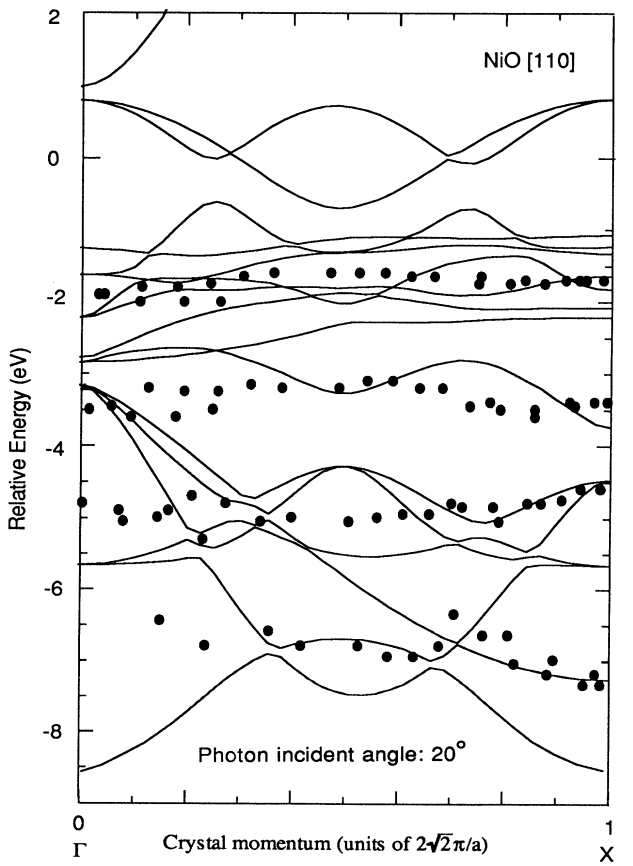

FIG. 22. Experimental E vs $\mathbf{k}$ relation from data in Fig. 20 in comparison with bands along [110].

ever, this will not affect our discussion, since only the relative energy is important here. There are two dominant satellite components separated by 1.5 eV which have been observed in the earlier angle-integrated photoemission data.[19,20]

First, let us look at the two sets of data along ⟨100⟩ in Fig. 23. One can see that the two data sets are very similar, even though the data in Fig. 23 have better statistics. As the photon energy and emission angle ratio is increased from 40/28° to 42/31.5°, the lower-binding-energy satellite B' shifts downwards to reach its minimum. It then moves upward again for photon energies higher than 42 eV. This indicates that a critical point is reached at a photon energy (emission angle) of 42

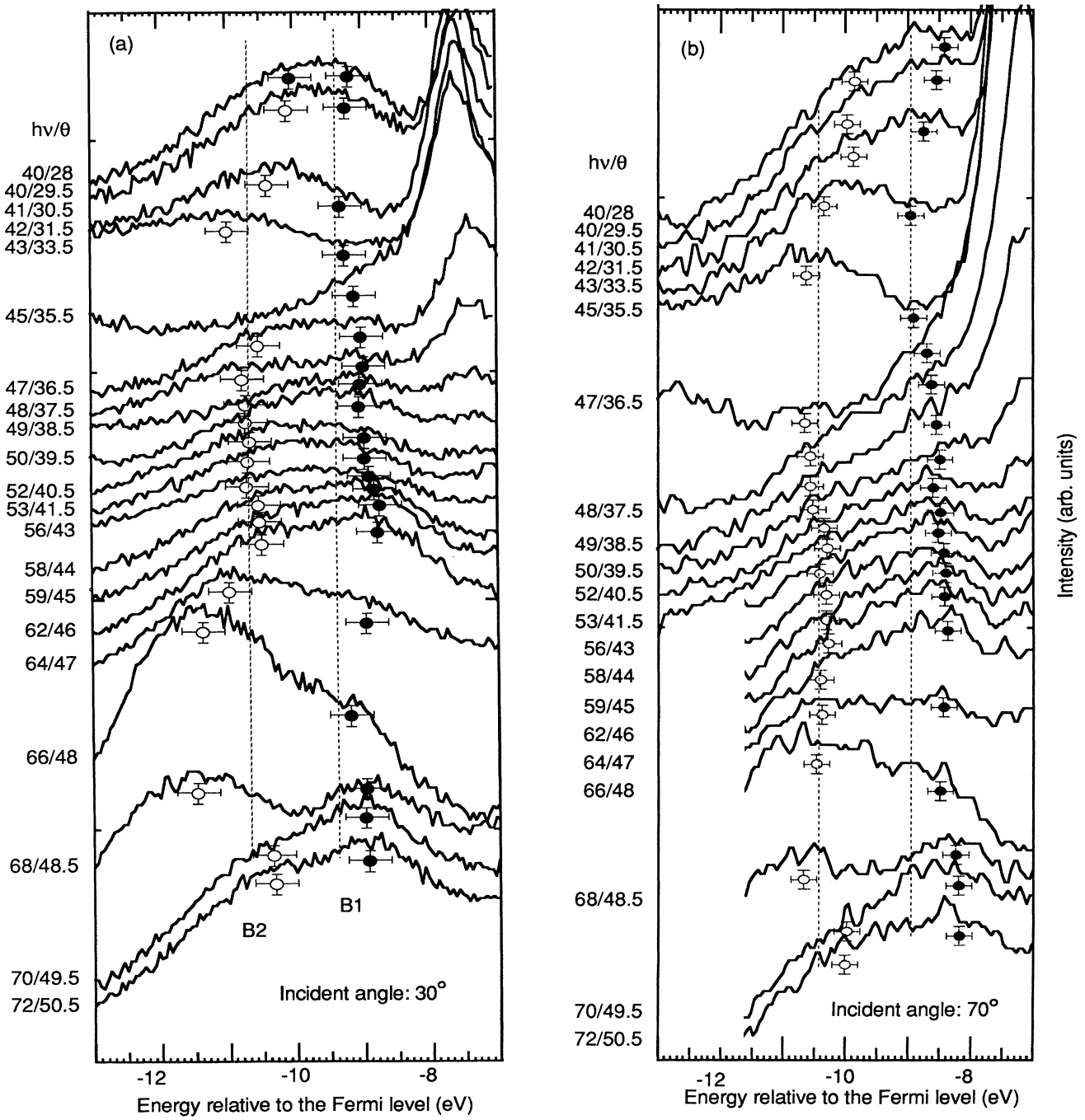

FIG. 23. (a) Satellite photoemission spectra along ⟨100⟩ with 30° photon incident angle. The numbers marked on each spectrum are photon energies and emission angles with respect to an ⟨100⟩ axis in the (100) surface. (b) Satellite photoemission spectra along ⟨100⟩ with 70° photon incident angle. The numbers marked on each spectrum are photon energies and emission angles with respect to an ⟨100⟩ axis in the (100) surface.

eV (31.5°). The crystal momentum calculated with the photon energy and the emission angle corresponds to the X point of the Brillouin zone, in agreement with the observed critical point. The higher-binding-energy component B'' shows a relative stronger downwards shift in the photon-energy range of 40–43 eV (40–45 in Fig. 23). Then there is a jump between the spectra taken at 43- and 45-eV photon energy (45–47 eV in Fig. 23), as if there is some type of resonance. Above 45-eV photon energy (47 eV in Fig. 23), feature B'' shifts less than feature B'. Both satellite components B' and B'' are affected by the Ni resonance for photon energies above 64 eV. This is most evident in the spectra of 66 and 68 eV. The resonance data indicates that there might be more than two components in the NiO satellite. But for the two components indicated, B' and B'', the latter shows stronger resonance. It should be pointed out that resonance data at 66- and 68-eV photon energies are not caused by an Auger peak sweep through the valence band.

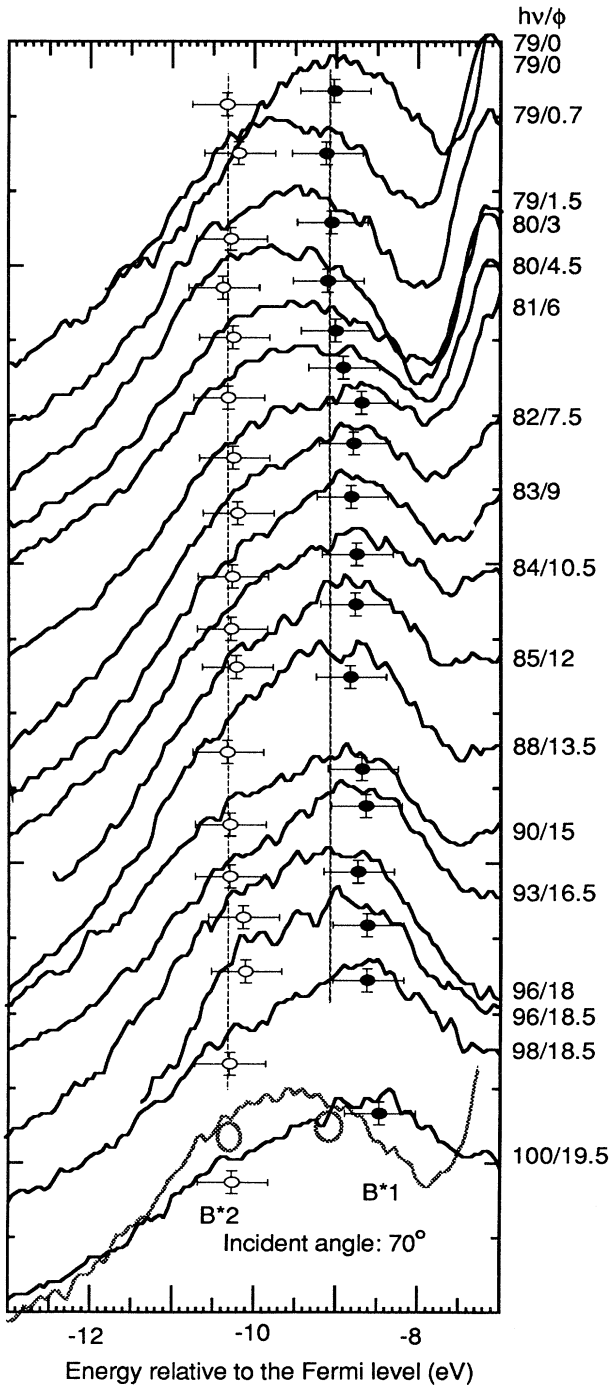

FIG. 24. Satellite photoemission spectra along ⟨110⟩ with 70° photon incident angle.

We now turn to the $B1$ satellite along ⟨110⟩. Here the photon energies chosen are well above the Ni $3p$-to-$3d$ threshold of 64 eV so that no influence of the resonances is involved. Similar to the data along ⟨100⟩, the lower-binding-energy component $B1'$ shows stronger dispersion. Going from the Γ point to the X point, the $B1'$ satellite shifts downwards by about 0.5 eV, while the satellite $B1'$ is basically flat except those near the X points. Since the d^7 final state has many crystal-field components, in principle we cannot rule out the possibility that what we see is actually relative intensity modulation instead of energy dispersion. To make the situation even worse, the satellite features are very broad, so that the error bar of the energy position is relatively large. However, we are convinced that our data is better interpreted by the satellite energy dispersion instead of relative intensity modulations for the following reasons. The upper curves with lower $h\nu/\phi$ values correspond to data close to the X point, while the lower curves with higher $h\nu/\phi$ values correspond to the results in the vicinity of the Γ point. As one goes from the upper curves to the lower curves, the whole satellite feature becomes broader. This is more clearly seen by stacking the topmost curve of 79/0 (gray line) on top of the lowermost curve of 100/19.5. If we now want to deconvolute the satellite into two components (which is suggested both by earlier angle-integrated-photoemission data and the angle-resolved-photoemission data along ⟨100⟩), the energy separation between the two components increases as one goes from the top curve to the bottom curve. This increase of the energy separation between the two components could in principle have two possible explanations: the energy dispersion and the relative intensity modulation. Since the photon energies we are using here are well above the Ni $3p$ absorption threshold of 64 eV, one would expect the photoionization cross sections of all the $3d$ states are very similar and are smooth functions of the photon energy. It would be hard to imagine by changing photon energy from 79 to 100 eV, the line shape of the $3d$ satellite will have as large a change as we have observed because of the relative intensity modulation. Therefore, the energy dispersion interpretation is most plausible.

The strongest piece of evidence which supports the energy-dispersion interpretation of our data is the systematics of our results. This is clearly shown in the experimental E vs $\mathbf{k}$ relations for the satellites in Fig. 25.

First of all, we approach the X point from the Γ point along two very different directions, $\langle 100 \rangle$ and $\langle 110 \rangle$, and get the same size of energy dispersion. For the two sets of data along $\langle 100 \rangle$ but with different photon incident angles, the energy dispersions of the satellites are very consistent and are well beyond the experimental error bars. Second, we are using very different photon energies for the data along $\langle 100 \rangle$ (see Fig. 23) and along $\langle 110 \rangle$ (see Fig. 24). It would have to be a coincidence if the same amount of movement of B' and $B1'$ satellites in both sets of data occurred because of the relative intensity modulations.

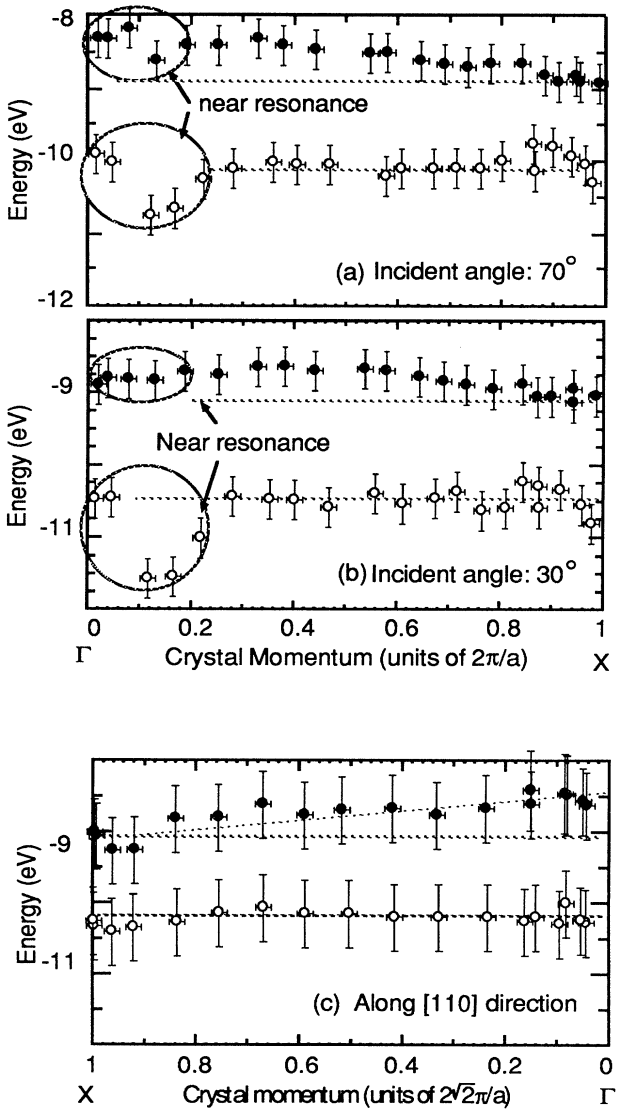

FIG. 25. Experimental E vs $\mathbf{k}$ relations for the satellite: (a) along [100] with photon incident angle of 70°, (b) along [100] with photon incident angle of 30°, (c) along [110] with photon incident angle of 70°. The component at higher energy shows about 0.5-eV dispersion. The component at lower energy is basically nondispersive except at few points near the X point. The data points circled are influenced by the Ni resonance.

Having convinced ourselves of the observation of the satellite dispersion, an interesting anticorrelation between the energy dispersion and the Ni resonance is obvious. The B' ($B1''$) satellite, which shows weaker resonance, has about 0.5-eV energy dispersion. On the other hand, the B'' (B') satellite, which exhibits much stronger resonance, is basically nondispersive. This anticorrelation is not related to the polarization of the incident photons: the E vs $\mathbf{k}$ relations deduced from the data in Fig. 23 are almost identical, even though the photon polarizations in the two data sets are very different. Another interesting observation is that the resonance behavior of the satellites in Fig. 23 is somewhat different from the angle-integrated resonance photoemission data which shows that both B' and B'' exhibit strong resonances (of course, the B'' resonance is also relatively stronger than that of B').

VII. DISCUSSION

As we have shown above, the angle-resolved-photoemission data from NiO provide additional information about the electronic structure of the compound. To the best of our knowledge, this is the first detailed comparison between angle-resolved-photoemission data and one-electron band calculation from a prototype of the Mott insulators. The message we get from out experimental data is that the excitation spectra of this compound have a dual nature. On the one hand, we can see that many aspects of the data agree with the LDA calculation well. On the other hand, we find that some of our data cannot be explained by the LDA calculation. Since one of the important motivations of the present work is to explore how well the LDA calculation can account for the electronic structure of NiO, and to what extent it fails, we organize our discussion along the line of comparison with the LDA calculation.

We start our discussion with the agreements between the experimental data and the LDA calculation. First of all, we can see that it is essential to include the antiferromagnetic order in the theoretical calculations. Even though the importance of the antiferromagnetic order to the band structure has been recognized theoretically for a long time,[12] this problem has never been explicitly addressed experimentally. It is interesting that these effects show up so clearly in our experiments, given the fact that the experimental probe is not spin sensitive. As clearly shown in the comparison between the nonmagnetic and the antiferromagnetic bands (see Figs. 6, 12, 13, and 16–18), the inclusion of the antiferromagnetic order improves the agreement between the experimental data and the LDA calculation significantly. This effect is most clearly seen for the Ni $3d$ bands. The antiferromagnetic $3d$ bands are much narrower than the nonmagnetic bands, thus improving the agreement with the experimental data. As shown in Figs. 6, 12, 13, and 17 the experimental data points fall on top of the theoretical $3d$ bands. Except in the energy range between E_F and the first experimental band, the general spread of the experimental $3d$ bands agrees with the antiferromagnetic LDA

bands quite well. In the energy range where the antiferromagnetic bands are heavily populated (e.g., from -1 to -2.5 eV in Fig. 13), we see three experimental bands. These three experimental bands spread out in an energy range which is very similar to the theoretical prediction. In the experimental data, we also observe a single Ni $3d$ band which is well separated from the rest of the Ni $3d$ bands. As shown in Figs. 6, 12, 13, and 17, there is a theoretical Ni $3d$ band separated from the rest of the Ni $3d$ bands which coincides in energy position with the experimental band.

For the oxygen $2p$ bands, the effect due to the antiferromagnetic order exists, but is not as evident as for the Ni $3d$ bands. This is not unexpected, since the antiferromagnetic order is formed on the moments sitting on the Ni sites. For the $\Delta 1$ oxygen band, there is an almost perfect agreement between the experiment and both the nonmagnetic as well as the antiferromagnetic band calculations. The discrepancies near the Γ point in the off-normal-emission data are mainly caused by the experimental uncertainties, as discussed earlier. The symmetry of this band is also verified by our polarization studies to be consistent with the theory. In the off-normal-emission data along $\langle 100 \rangle$, we observe an extra oxygen band in the energy range of the $\Delta 5$ band if we do not consider the antiferromagnetic order. We believe this extra band is due to the folded-back band from the $(\pi/a)\langle 111 \rangle$ to $(\pi/a)\langle 311 \rangle$ symmetry directions as a result of the antiferromagnetic order. However, the energy position of this band is somewhat off. This folded-back band is not as clearly seen in the normal emission data (Fig. 6). It appears that the effects of the antiferromagnetic order on the oxygen bands are more clearly seen in the ones that have higher energy and are closer to the Ni $3d$ bands. For example, the antiferromagnetic folded-back band near -8 eV has never been clearly seen in the experimental data. This may be related to the fact that these oxygen $2p$ bands are more heavily hybridized with the nickel $3d$ bands so that they feel the effect of antiferromagnetic order on the nickel sites more strongly. The fact that the effects of the antiferromagnetic order can sometimes by seen more clearly than others is consistent with an earlier LEED study of NiO.[55] Because the magnetic lattice of the NiO (100) surface has twice the dimension of the crystal lattice, one would expect to see the half-order diffraction patterns. Indeed, such half-order diffraction patterns have sometimes been seen in the LEED experiments at 80 °C.[55]

In this paragraph, we discuss the energy separation between Ni $3d$ and O $2p$ bands. This turns out to be a tricky issue. An earlier comparison of LDA calculation and angle-integrated-photoemission data suggest that the LDA calculation gives an energy separation which is 2 eV too large.[52] The comparison of the LDA calculation and our angle-resolved-photoemission data gives a more complicated picture. Along the $\langle 100 \rangle$ direction, if we only look at energy positions, then LDA gives the correct energy separation between the Ni $3d$ and O $2p$ bands. On the other hand, if we look at the intensity of the peaks, it is not so straightforward anymore. Even though there is a theoretical band near -3 eV (Figs. 6, 12, and 13) corresponding to the experimental band C, it may not be enough to account for the relatively high intensity of feature C in the data. According to the theory, there are many bands in the energy range of feature A, while there is only one band in the energy range of feature C. However, one does not see that the emission intensity of feature A is much higher than that of feature C (though the data suggests that feature A has several components). The emission intensity of the angle-resolved data is very hard to quantify so that the seemingly too high intensity of the feature C is still an open question. A similar conclusion can also be drawn for the data along $\langle 110 \rangle$ with few differences. The agreement between the theory and the experiment on feature C is even worse along $\langle 110 \rangle$. Furthermore, the theory predicted something between 0 and -1 eV along $\langle 110 \rangle$ which is not observed in the experiment. Therefore, the angle-resolved data give the following picture: If we match the energy positions of the theoretical and the experimental oxygen bands, we then find data points fall on the energy range where there are theoretical Ni $3d$ bands. However, the relative intensity of various $3d$ bands is still an open question. This result is certainly different from the 2-eV shift scenario proposed earlier.[52] Three possible reasons are the following: (a) When Kübler and Williams compared the LDA result and the angle-integrated data, they tried to give the best intensity match also. Hence the matching criteria in their approach was slightly different from that of ours. (b) If one looks at the analysis of Kübler and Williams (see Fig. 3 of Ref. 52), one finds that the energy separation between the Ni $3d$ and O $2p$ bands is about 1 eV too small as compared with the experimental data after they shift the Ni $3d$ bands down by about 2 eV (check the O $2p$ band noted by σ, for example). (c) Previous angle-integrated-photoemission data taken with a cylindrical mirror analyzer (CMA) could be quite different from the total density of states. After all, the data taken with CAM was not truly angle integrated. Furthermore, the experimental spectrum should be the *coherent summation* of the partial density of states weighted by photoioinization cross sections.

Now, we turn our attention to the disagreements between our experimental data and the band calculation. There are two major discrepancies. The first one is the absence of the theoretical bands just below E_F in the experimental data. As shown in Figs. 6, 12(b), 13, and 17, there are always theoretical bands in the energy range between E_F (pinned position of the Fermi level) and the first-observed Ni $3d$ band (usually near -1 eV). Since we have many different sets of experimental data which were taken with very different experimental geometries, it seems impossible for these bands to be invisible by selection rules. These are the theoretical bands that should be empty if we count the number of electrons. Obviously, since their predicted energy positions are wrong, they are below the experimental Fermi level. Therefore, this discrepancy is related to the fact that the LDA calculations cannot reproduce the experimental gap value of NiO. The best gap value of the LDA calculation for NiO is 0.2 eV by Terakura and co-workers,[13] which is an order of magnitude smaller than the experimental gap value of

about 4 eV.[15,16] On the other hand, the absence of the antiferromagnetic folded-back oxygen band near -8 eV may be explainable by the fact that the effects due to the antiferromagnetic order on the oxygen band are weak.

The second major discrepancy is the observation of the photoemission satellite which cannot be predicted by the LDA calculation. This satellite is often explained in terms of the d^7 final state, which is pushed to high energy due to the strong on-site Coulomb interaction, U.[16,17] The existence of the Ni $3d$ valence-band satellite is thus usually regarded as a strong piece of evidence which demonstrates the importance of correlation effects.

In addition to the two major discrepancies, we have also observed disagreements between the details of the angle-resolved-photoemission data and the band theory. Even though the general energy spread of the Ni $3d$ bands is very similar for theory and experiment, the dispersion of the individual bands in the experiment may be narrower than that of the theory. This can be most clearly seen in the small energy dispersion of feature C (see Figs. 6, 12, 13, and 17), which is well separated from the other bands so that a direct comparison becomes possible. If our identification of feature C is correct, this lack of dispersion for feature C implies that the LDA calculation overestimates the overlap between the Ni $3d$ bands. This result is also related with the observed discrepancy between the energy positions of the calculated and measured back-folded O $2p$ band ($+$ band in Figs. 12 and 13). The energy position of this band in the experiment is much higher than in the theory. It turns out that this band has substantial Ni character because of hybridization. Therefore, it is conceivable for this band to be pushed down too much by the LDA calculation which overestimates the hybridization between $3d$ and $2p$ states. The p-d hybridization can be reduced by narrowing the d band. A separate calculation with an artificially reduced d-band width indeed moved the folded-in p bands up relative to the unfolded bands. In addition to its energy position, the experimental energy dispersion of this oxygen $2p$ (but mixed with Ni $3d$) band does not agree with the theory. The theory suggests that this band should be very flat, but the experimental data show that the two branches of the band on either sides of the $\Delta 1$ bands are at very different energy positions. Of course, it is difficult to rule out the possibility that these are two independent bands.

Considering the above discussion, it is clear that there is some agreement between our experimental data and the LDA calculation. In other words, in addition to its success in providing some useful information about the ground-state properties, the LDA calculation also provides some useful information about the electronic structure of NiO. This is especially true for the oxygen bands, even though one can also learn something about the Ni bands from the LDA calculation. The agreement for the lowest oxygen E (●) band is really striking, and is even better than for the bands in the simple metals like Na and K.[56] If we consider the oxygen bands as full bands, then maybe it is not so difficult to understand this observation, since the correlation effects are no longer relevant in the full-band case. However, since the O $2p$ bands are strongly mixed with the $3d$ bands, it is no longer clear that they should be regarded as full bands anymore.

To first order, the result seems to suggest that the major problem for the LDA calculation is that it predicts unobserved spectral weight in the gap region but not the observed spectral weight in the satellite region. Otherwise, the antiferromagnetic LDA calculation gives a reasonable picture for the band structure of NiO. This in some sense has similarities to the case of Ni metal where a Ni satellite is also observed. The satellite in Ni metal is explained in terms of the two-hole bound state.[57] The difference between NiO and Ni metal is the gap problem.

We would also like to take this opportunity to emphasize again the consistencies in the experimental results presented in this paper. This is most clearly demonstrated in the data along $\langle 100 \rangle$. During the experiment, the photon energy, kinetic energy, and the emission angle of the photoelectrons are directly measurable quantities. From these quantities, we can deduce the crystal momentum by assuming a free-electron final-state approximation. As we have pointed out in Sec. II, the formulas to obtain $\mathbf{k}$ values in the normal emission and off-normal emission are very different. The fact that we see such a consistent picture from both the normal-emission and the off-normal-emission data makes us very confident with our interpretation of the data.

We believe our result obtained from this study is not limited to NiO, but is generally true for the later transition-metal mono-oxides—prototypes of the Mott insulators. This speculation has been confirmed by some preliminary angle-resolved-photoemission studies of CoO.[22] In the CoO case, because the broadening effects of the CoO $3d$ bands are more severe, fewer details can be learned about the $3d$ bands. However, for the lowest oxygen band along $\langle 100 \rangle$ ($\Delta 1$ symmetry), the LDA calculation again gives good agreement with the experiment. Furthermore, the experimental energy separation between the $2p$ and $3d$ bands is larger in CoO than in NiO, in agreement with the LDA band calculation. In other words, the LDA calculation gives a good relative energy between the O $2p$ and Ni $3d$ bands. Similarly, the antiferromagnetic order is found to be essential to the band structure of CoO. This is true even slightly above the Neel temperature, which is believed to be due to the local magnetic order. On the other hand, similar discrepancies between the experiment and the LDA calculation are also found in CoO. We are in the process of performing more studies of Mott insulator so that a larger data base can be generated. Angle-resolved photoemission studies of CoO have also been performed by Brooks *et al.*,[46] where they compared the experimental data with the results of earlier non-self-consistent paramagnetic bands.[40] Lad and Henrich have also performed angle-resolved-photoemission studies on MnO [100], and they did not observe strong energy dispersions as we observed in NiO [100].[58] However, they acknowledged later that the surface they studied may be affected by impurities.[59] Therefore, more studies on these oxides are required to understand the systematics of the band effects in the transition-metal mono-oxides.

Finally, we examine to what extent our data can be ex-

plained by the theoretical approaches other than the one-electron band calculation. The most popular model for NiO (and other transition-metal oxides) is the cluster version of the Anderson Hamiltonian proposed by Sawatzky and Allen[16] and Fujimoria and Minami.[17] Because this model is a cluster version, we cannot get any information about the energy dispersion. The main advantage of this model is that it can explain the satellite structure very nicely. Within the framework of this model, the satellite is the d^7 final state been pushed to high "binding" energy. With appropriate fitting parameters, this model is expected to reproduce the gap information, the general energy spread of the $3d$ band, as well as the energy separation between the $2p$ and $3d$ bands. However, since it is just a model calculation, it is not realistic enough to enable a direction comparison between the calculation and our angle-resolved-photoemission data.

It is also appropriate here to point out an often misunderstood point about the cluster model for NiO. In the cluster model, without considering the p-d hybridization, the Ni $3d$ band is split into upper and lower Hubbard bands with the lower Hubbard band completely filled. The oxygen bands are located between the two Hubbard bands and are filled, thus forming the charge transfer gap with the upper Hubbard band. If one takes this picture naively, then he will find this is inconsistent with our angle-resolved-photoemission data which show that the Ni bands are above the O bands. In this picture, the occupied oxygen bands are located at lower binding energy than the occupied nickel bands. This paradox can be easily explained if one considers the hybridization between the O $2p$ and the Ni $3d$ states. Due to the hybridization, the oxygen states that are very strongly hybridized with the nickel states are pushed up. The cluster calculations actually showed that bound states with mixed $d^8\underline{L}$, $d^9\underline{L}^2$, and d^7 characters are pushed out. Therefore, for the oxygen bands, the upper part has more Ni $3d$ character so that these bands are localized. The lower part has less $3d$ character so that these bands are more dispersive. The lower Hubbard band is located at even higher binding energy in the form of the satellite. In the same context, we want to emphasize that the bands which we called d bands in our comparison with the LDA calculation are actually the bound states in the cluster picture. These bands in our data can either be interpreted at the d bands of the LDA calculation or the bound states of the cluster calculation. We called those bands d bands in this paper only because we were comparing our data with the LDA calculation. It is easier for comparison to use the LDA language.

Recently, new theoretical efforts have been made to understand the electronic structure of NiO.[60–62] Svane and Gunnarsson have developed a self-interaction-corrected density-functional formalism for the transition-metal oxides in which they were able to include the localized nature of the $3d$ bands more explicitly.[60] As a result, they can correctly reproduce that MnO, FeO, CoO, NiO, and CuO are antiferromagnetic insulators, and that VO is a nonmagnetic metal. Furthermore, the calculated band-gap values are drastically improved as compared with the LDA calculation. It is interesting to note that they can only get good results with extended bands like oxygen $2p$ states. They cannot minimize the total energy of the system if the oxygen states are also localized. This general finding of the theory is consistent with the dual nature of the electronic structure of NiO found in our experiment. However, the relative energy separation between $2p$ and $3d$ bands and its comparison with experimental data are still open questions.

We hope our experimental work will stimulate more such theoretical efforts to incorporate the correlation effects into the band calculations, or to extend the cluster model into the real lattice model.

VIII. CONCLUSIONS

We conclude this work with the following remarks: Based on a detailed comparison between angle-resolved-photoemission data and the LDA calculation, we have found a dual nature for the electronic structure of NiO. On the one hand, the LDA band calculation certainly has some relevance to the electronic structure of NiO, and the inclusion of the antiferromagnetic order in the calculation is essential. For the lower O $2p$ bands, the antiferromagnetic LDA calculation agrees almost perfectly with the experimental energy positions and the dispersion relations. On the other hand, discrepancies between our data and the LDA calculation clearly exist, and they seem to be concentrated on the energy regions of the "insulating gap" and the satellite.

ACKNOWLEDGMENTS

It is a great pleasure to acknowledge the helpful discussions with Professor W. E. Spicer, Professor I. Lindau, Professor G. A. Sawatzky, and Professor J. W. Allen. Part of the experiment was performed at SSRL, which is funded by the U.S. Department of Energy under Contract No. DE-AC03082ER-13000. Experimental data were also collected at SRC and NSLS. The studies at Stanford are supported by U.S. National Science Foundation Contract No. DMR-89103478, U.S. Joint Service Electronics Program Contract No. DAAG29-85-K-0048, and a Grant through the Center at Material Research at Stanford. D.S.D. acknowledges support from NSF.

[1]Z.-X. Shen, C. K. Shih, O. Jepsen, I. Lindau, W. E. Spicer, and J. W. Allen, Phys. Rev. Lett. **64**, 2442 (1990).

[2]Z.-X. Shen *et al.*, Solid State Commun. (to be published).

[3]P. W. Anderson, in *Frontier and Borderlines in Many Particle Physics,* Proceedings of the International School of Physics "Enrico Fermi," Course CIV, edited by R. A. Broglia and J. R. Schrieffer (North-Holland, Amsterdam, 1988).

[4]B. H. Brandow, Adv. Phys. **26**, 651–808 (1977).

[5]J. W. Allen, in *Narrow Band Phenomena—Influence of Electrons with both Band and Localized Character,* Vol. 184 of *NATO Advanced Study Institute, Series B: Physics,* edited by J. C. Fuggle, G. A. Sawatzky, and J. W. Allen (Plenum, New

York, 1988), p. 155.
[6]J. C. Slater, *Quantum Theory of Molecules and Solids* (McGraw-Hill, New York, 1965).
[7]O. Madelung, *Introduction to Solid-State Theory* (Springer-Verlag, Berlin, 1981).
[8]W. A. Harrison, *Solid State Theory* (Dover, New York, 1979).
[9]P. W. Anderson, Phys. Rev. **115**, 2 (1959).
[10]N. F. Mott, Proc. R. Soc. London Ser. A **62**, 416 (1949).
[11]J. Hubbard, Proc. R. Soc. London Ser. A **276**, 238 (1963).
[12]J. C. Slater, Phys. Rev. **82**, 538 (1951).
[13]K. Terakura, T. Oguchi, A. R. Williams, and J. Kübler, Phys. Rev. B **30**, 4734 (1984); T. Oguchi, K. Terakura, and A. R. Williams, *ibid.* **28**, 6443 (1983).
[14]M. R. Norman, Phys. Rev. Lett. **64**, 1162 (1990).
[15]R. J. Powell and W. E. Spicer, Phys. Rev. B **2**, 2182 (1970).
[16]G. A. Sawatzky and J. W. Allen, Phys. Rev. Lett. **53**, 2339 (1985).
[17]A. Fujimori and F. Minami, Phys. Rev. B **30**, 957 (1984).
[18]D. E. Eastman and J. L. Freeoff, Phys. Rev. Lett. **34**, 395 (1975).
[19]S.-J. Oh, J. W. Allen, I. Lindau, and J. C. Mikkelsen, Jr., Phys. Rev. B **26**, 4845 (1982).
[20]M. R. Thüler, R. L. Benbow, and Z. Hurych, Phys. Rev. B **27**, 2082 (1983).
[21]K. S. Kim, Phys. Rev. B **11**, 2177 (1975); Chem. Phys. Lett. **26**, 234 (1974).
[22]Z.-X. Shen, J. W. Allen, P. A. P. Lindberg, D. S. Dessau, B. O. Wells, A. Borg, W. Ellis, J. S. Kang, S.-J. Oh, I. Lindau, and W. E. Spicer, Phys. Rev. B **42**, 1817 (1990).
[23]M. R. Thüler, R. L. Benbow, and Z. Hurych, Phys. Rev. B **26**, 699 (1982).
[24]G. K. Wertheim, H. J. Guggenheim, and S. Hüfner, Phys. Rev. Lett. **30**, 1050 (1973); G. K. Wertheim and S. Hüfner, *ibid.* **28**, 1028 (1982).
[25]A. Fujimori, N. Kimizuka, M. Taniguchi, and S. Suga, Phys. Rev. B **36**, 6991 (1987).
[26]J. Zannen, G. A. Sawatzky, and J. W. Allen, J. Magn. Magn. Mater. **54-57**, 607 (1986).
[27]G. van der laan, C. Westra, C. Haas, and G. A. Sawatzky, Phys. Rev. B **23**, 4369 (1981).
[28]K. E. Smith and Victor E. Henrich, Phys. Rev. B **38**, 5965 (1988).
[29]L. C. Davis, J. Appl. Phys. **59**, R25 (1986).
[30]B. H. Brandow, Solid State Commun. **69**, 915 (1989).
[31]A. Fujimori, N. Kimizuka, M. Taniguchi, and S. Suga, Phys. Rev. B **36**, 6691 (1987).
[32]Z.-X. Shen, J. W. Allen, J. J. Yeh, J. S. Kang, W. Ellis, W. E. Spicer, I. Lindau, M. B. Maple, Y. D. Dalichaouch, M. S. Torikachivili, J. Z. Sun, and T. H. Geballe, Phys. Rev. B **36**, 8414 (1987).
[33]J. C. Fuggle, P. J. W. Weijs, R. School, G. A. Sawatzky, J. Fink, N. Nücker, P. J. Durhan, and W. M. Temmerman, Phys. Rev. B **37**, 123 (1988).
[34]P. A. P. Lindberg, Z.-X. Shen, W. E. Spicer and I. Lindau, Surf. Sci. Rep. **11** (1–4), 1 (1990), and references therein.
[35]See, e.g., *Materials and Mechanisms of Superconductivity, High Temperature Superconductors II,* edited by R. N. Shelton, W. A. Harrison, and N. E. Phillips (North-Holland, Amsterdam, 1989).
[36]Mckay and Henrich have performed semi-angle-resolved photoemission studies on NiO [100]: Jeffrey M. Mckay and Victor E. Henrich, Phys. Rev. Lett. **53**, 2343 (1980). We call this a semi-angle-resolved study because the angular resolution of the experiment was very poor (±6° for polar angle and ±40° for azimuthal angle).
[37]U. von Barth and L. Hedin, J. Phys. C **5**, 1629 (1972).
[38]O. K. Andersen, Phys. Rev. B **12**, 3060 (1975).
[39]O. K. Andersen, O. Jepsen, and D. Götzel, in *Highlights of Condensed Matter Physics,* Proceedings of the International School of Physics "Enrico Fermi," Course LXXXIX, edited by F. Bassani, F. Fumi, and M. P. Tosi (North-Holland, Amsterdam, 1985).
[40]L. F. Matheiss, Phys. Rev. B **5**, 290 (1972).
[41]N. V. Smith and F. J. Himspel, in *Handbook on Synchrotron Radiation,* edited by E.-E. Koch (North-Holland, Amsterdam, 1983), Chap. 9.
[42]R. Courths and S. Hüfner, Phys. Rep. **112**, 53 (1984).
[43]F. J. Himpsel, Adv. Phys. **32**, 1 (1983).
[44]T. C. Chiang, J. A. Knapp, D.E. Eastman, and M. Aono, Solid State Commun. **31**, 917 (1979).
[45]J. C. Hwang, Ph.D. thesis (Stanford University, 1989).
[46]N. B. Brooks, D. S.-L. Law, D. R. Warburton, P. L. Wincott, and G. Thornton, Phys. Condens. Matter **1**, 4267 (1989).
[47]R. C. Felton, M. Prutton, S. P. Tear, and M. R. Welton-Cook, Surf. Sci. **88**, 474 (1979).
[48]J. Hermanson, Solid State Commun. **22**, 9 (1977).
[49]W. Eberhardt and F. J. Himpsel, Phys. Rev. B **21**, 5572 (1980).
[50]The 2′ band should not be observable at normal emission if the accept angle of the analyzer is infinitely small.
[51]J.-J. Yeh and I. Lindau, At. Data Nucl. Data Tables **32**, 1 (1985).
[52]J. Kübler and A. R. Williams, J. Magn. Magn. Mater. **54-57**, 603 (1986).
[53]G. A. Sawatzky, Phys. Rev. Lett. **39**, 504 (1977).
[54]P. Ricebourough (private communication).
[55]F. P. Netzer and M. Prutton, J. Phys. C **8**, 2401 (1975).
[56]H.-J. Freund, W. Eberhardt, D. Heskett, and E. W. Plummer, Phys. Rev. Lett. **50**, 768 (1983); In-Whan Lyo and E. W. Plummer, *ibid.*, **60**, 1558 (1988).
[57]A. Liebsch, Phys. Rev. Lett. **43**, 1431 (1979).
[58]Robert J. Lad and Victor E. Henrich, Phys. Rev. B **38**, 10 860 (1988).
[59]Shin-Puu Jeng, Robert J. Lad, and Victor E. Henrich (unpublished).
[60]G. A. Sawatzky, in *On the Electronic Structure and Related Physical Properties of* 3*d Transition Metal Compounds,* edited by J. G. Bednorz and K. A. Muller, Springer Series in Solid State Sciences Vol. 90 (Springer, Berlin, 1989).
[61]A. Svane and O. Gunnarsson, Phys. Rev. Lett. **65**, 1148 (1990).
[62]V. I. Anisimov, J. Zaanan, and O. K. Andersen, Phys. Rev. B **44**, 943 (1991).